Last Glacial Maximum Climate and Atmospheric Circulation over the Australian Region from Climate Models

Yanxuan Du[1], Josephine R. Brown[1], J. M. Kale Sniderman[1]

[1] School of Geography, Earth and Atmospheric Sciences, University of Melbourne, Parkville, VIC, Australia

5 *Correspondence to*: Yanxuan Du (yanxuand@student.unimelb.edu.au)

Abstract. The Last Glacial Maximum (LGM, ~21,000 years ago) was the most recent time that the Earth experienced global maximum ice volume and minimum eustatic sea level. The climate changes over the Australian region at the LGM remain uncertain. In this study, five Coupled Model Intercomparison Project Phase 6 (CMIP6) models and eight Coupled Model Intercomparison Project Phase 5 (CMIP5) models that were included in the Paleoclimate Modelling Intercomparison Project

10 (PMIP) Phases 3 and 4 are used to investigate regional climate (temperature, precipitation, and wind) over Australia at the LGM. The model simulations are compared with existing proxy records and other modelling studies. All models simulate consistent annual and seasonal cooling over the Australian region (defined as 0-45°S, 110°E-160°E) with a multi-model mean 2.9°C decrease in annual average surface air temperature over land at the LGM compared to pre-industrial. While models show consistent patterns of regional cooling over Australia at the LGM, the changes in precipitation differ between

15 models. The simulated precipitation changes over tropical Australasia appear to be driven by changes in circulation and moisture transport, which vary greatly between models. Surface moisture balance calculated from precipitation minus evaporation shows little change over much of the Australian land area at the LGM. Changes in the strength and position of the mid-latitude westerlies are also uncertain, with wide model disagreement. These results indicate that climate models do not have a robust response in either tropical or mid-latitude circulation to LGM boundary conditions, suggesting that caution

20 is required when using output from a single model in this region. Further analysis is required to determine the drivers of model circulation changes in this region and to identify the most plausible set of LGM simulations before quantitative model-proxy comparison can be attempted.

1 Introduction

The Last Glacial Maximum (LGM, ~21,000 years ago) refers to the coldest interval within the last glacial period, featuring

25 global maximum ice volume and associated low eustatic sea-level (Clark et al., 2009). Ice sheets covered large parts of North America, Europe, and Northern Eurasia at this time (Ehlers and Gibbard, 2007). In Australia, Reeves et al. (2013a) present evidence of small glaciers in the Snowy Mountains of southeast Australia and Tasmania, with the most significant glacier advance at around 19.1 ka (Petherick et al., 2013). Global mean surface air temperature (SAT) estimates during the LGM range from 3.4 to 8.3 °C cooler than pre-industrial based on different model ensemble results constrained with proxy data

30 (Schneider von Deimling et al., 2006; Holden et al., 2010; Annan and Hargreaves, 2013; Tierney et al., 2020a; Seltzer et al.,

2021; Annan et al., 2022) with recent studies suggesting a narrower range of 4.5 °C ± 0.9 °C (Annan et al., 2022) or 5.7 °C to 6.5 °C (Tierney et al., 2020a) depending on the method used. The global sea level was estimated at ca.120 meters lower than today (Lambeck et al., 2014; Yokoyama et al., 2018), resulting in the expansion of the land areas in many parts of the world, appearance of land bridges and the exposure of Sunda and Sahul shelves in Southeast Asia, which further allowed

35   human migration during this period (Clarkson et al., 2017). The Australian mainland expanded at the LGM, connected by land bridges to New Guinea, Tasmania, and many smaller islands into a single landmass known as "Sahul" (Clarkson et al., 2017, see Figure 1 with the grey shading covering the land areas).
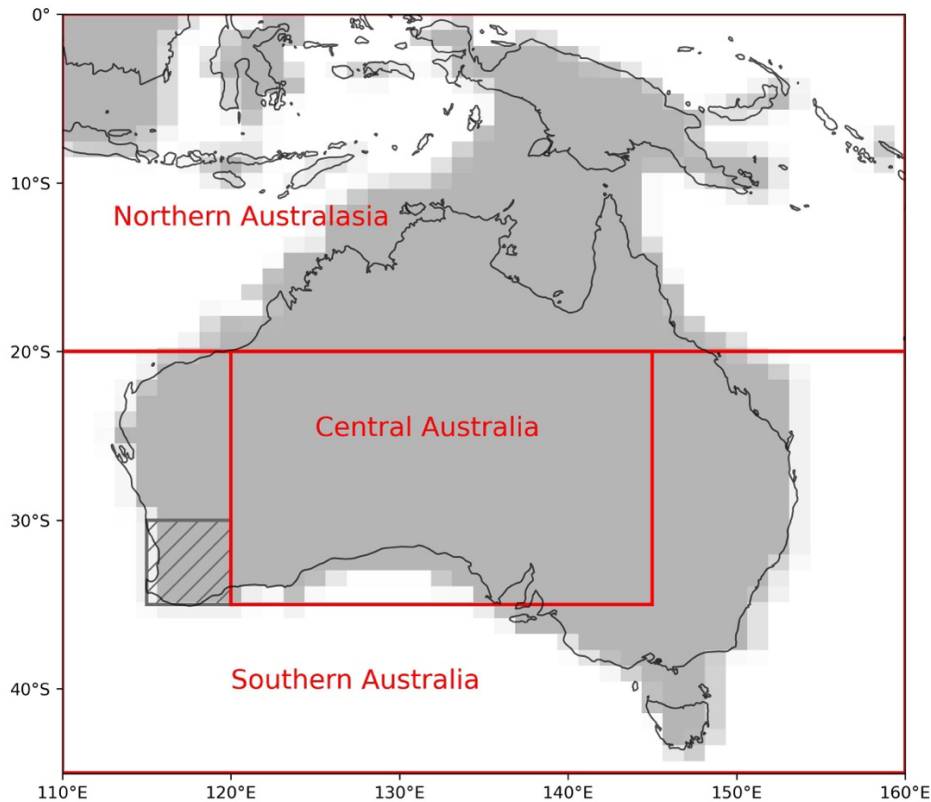
40   **Figure 1:** Classification of Northern Australasia, Central, and Southern Australia domains shown by red rectangles with modern day coastlines. The Central Australia domain is a subset of the larger Southern Australia domain. The south-west box for detecting JJA frontal precipitation that is most sensitive to westerlies is also indicated in hashes in the Southern Australia domain. The background grey shading indicates LGM land mask from CCSM4 model, plotted over modern coastlines.

45   LGM vegetation was also very different from today. There was a large reduction in area covered by boreal and temperate forests in northern mid- to high latitudes, expanded lowland tundra in Eurasia, expansion of savanna and grasslands at the margin of Amazon tropical forests and replacement of some areas of tropical forest in Africa, China and Southeast Asia with savanna, woodland and grassland (Prentice et al., 2011). These changes are associated with large LGM

reduction in terrestrial biomass, caused by a combination of lower temperatures, changes in hydroclimate (moisture availability), and/or lower atmospheric CO_2 concentrations (~180 ppm) that cooled the climate and restricted vegetation growth (Scheff et al., 2017; Prentice et al., 2022). Dust suspension and transport was estimated to be more active at the LGM, which was possibly driven by stronger winds and drier climate conditions, particularly in the tropical and high-latitude regions (Lamy et al., 2014), or may have been partly a consequence of the reduced ability of terrestrial vegetation to stabilize soils (Scheff et al., 2017; Roderick et al., 2015).

The LGM is commonly recognised as a time of global cooling and lower sea levels, best estimates placing this at ca. 21 ka (Hughes et al., 2013). However, changes in Southern Hemisphere (SH) regional temperature, rainfall and atmospheric circulation are less well understood. In the SH, on landmasses remote from continental ice sheets, it has become clear from pollen and other terrestrial climate proxies that full glacial conditions were maintained in New Zealand and Australia between ca. 28-18 ka (Newnham et al., 2007; Cadd et al., 2021), which Newnham et al. (2007) referred to as the 'extended LGM'. Understanding the changes in regional climate over Australia at the LGM is of interest for a number of reasons. The Australian climate is influenced by major tropical and extratropical modes of circulation, including the Walker circulation and SH Hadley Cell, Indo-Australian monsoon and mid-latitude westerlies. Therefore, understanding how the climate of Australia changed at the LGM could provide insight into the changes in these large-scale climate processes. In addition, it is also crucial for interpreting records of human occupation (Williams et al., 2013; Bird et al., 2016; Bradshaw et al., 2021) and changes in flora and fauna distributions (Byrne et al., 2008; Nevill et al., 2010; Pepper and Keogh, 2021) from this period.

A limited number of climate modelling studies have focused on conditions during the LGM in the SH (e.g. Rojas et al., 2009; Rojas, 2013; Sime et al., 2013), with even fewer studies examining simulations of LGM climate in Australia (e.g. Hope, 2005; Yan et al., 2018). Some studies (e.g. Brown et al., 2020; Kageyama et al., 2021; Wang et al., 2023) have begun to explore the new PMIP4 simulations of LGM climate, but there has been little research on the changes in SH climate, including the Australian region in these simulations (or the older PMIP3 ensemble). This study investigates the climate (temperature, precipitation, moisture balance and wind) changes during the LGM relative to PI over the Australian region using available simulations from PMIP3/PMIP4 models and compares the results with existing proxy records and other model studies of the region. The aim is to provide preliminary insights into the LGM climate in Australia from model simulations and evaluate the model consistency with available proxy records.

1.1 Palaeoenvironmental proxy records for the Australian LGM

This section summarises the available proxy records across the Australian region separated into three distinct climate zones (see Figure 1 and Section 2.3 for the classification and map) from the period 24 to 18 ka as broadly representative of LGM reconstructed climate in Australia. The regional comparisons with our model simulation results are presented in the Discussion (Section 4).

In northern Australia (see Figure 1 for corresponding region), surrounding sea surface temperatures (SSTs) are estimated to have cooled by 1 to 3 °C at the LGM relative to present (Reeves et al., 2013a). The temperature in upland areas in New Guinea is estimated to have reduced by 4 to 6 °C compared to present based on pollen records from near treeline in the Kosipe Valley (Hope, 2009). A dramatic reduction in tree cover was identified at the LGM in tropical savanna woodland in northern Australia from pollen and geochemical records (Rowe et al., 2021). Rowe et al. (2021) attributed the change in vegetation to a combination of a cooler and drier glacial climate, while also considering the possible role of lower atmospheric CO_2 concentrations and the increased distance of the site from the coastline. Reduced fire activity occurred as a result of less available fuel, indicating that the vegetation at the LGM was less influenced by fire events than today (Rowe et al., 2021). There is uncertainty about the drivers of LGM climate changes in northern Australia; sparser vegetation has been interpreted previously as a sign of aridity, but it is also likely that low CO_2 played a role in reducing plant biomass (e.g. Scheff et al., 2017; Prentice et al., 2017; Prentice et al., 2022). Denniston et al. (2013) found evidence of an active but variable monsoon during the LGM based on speleothem records at Ball Gown Cave in tropical northern Australia, with more positive speleothem isotopic values at the LGM than the late Holocene indicating relatively dry glacial conditions.

In southern Australia during the LGM, a SAT reduction of 4-6 °C has been inferred from pollen records, and SST cooling varying from 3 to 9 °C has been inferred in nearby ocean regions (Petherick et al., 2013). Fossil pollen records indicating widespread reductions in tree cover have often been interpreted as implying drier conditions, i.e. reduced precipitation and/or increased evaporation (Petherick et al., 2013), but the potential role of low atmospheric CO_2 in reducing plant productivity has rarely been considered in the region (Prentice et al., 2017; Sniderman et al., 2019). Moreover, regionally wetter conditions (increased precipitation and/or reduced evaporation) were also present in some parts of the Southern Australian domains (Reeves et al., 2013b), perhaps consistent with a northward shift of the SH westerlies at the LGM (Kohfeld et al., 2013). Some evidence of higher lake (Lakes Mungo, Keilambete and George) and river levels in the Murray-Darling Basin (Hesse et al., 2018) has been interpreted in terms of greater seasonal runoff due to snowmelt (Petherick et al., 2013), or some combination of higher precipitation and lower evapotranspiration (Hesse et al., 2018). In subtropical eastern Australia, the persistence of moisture-demanding woodlands suggests that the effective precipitation (net moisture) levels did not drop dramatically during the LGM in this region (Cadd et al., 2018).

In central Australia, the average LGM air temperature in the arid zone was estimated to decrease by 9 °C below present (Miller et al., 1997) based on amino-acid racemisation of emu eggshell. Fitzsimmons et al. (2013) argued that the arid interior experienced extensive dune activity and dust transport, reduced but episodic fluvial activity at the LGM relative to PI. However, there is geomorphological evidence for higher lake levels at Lake Frome (Cohen et al., 2015). Evidence of wetter conditions in arid Australia during the LGM was found by Treble et al. (2017) from speleothem records at Mairs Cave, Flinders Ranges in the Southern Australian semi-arid zone. That study suggested that the Flinders Ranges were relatively wet during the LGM, possibly associated with a southward shift of the Intertropical Convergence Zone (ITCZ), allowing more tropical moisture to reach the cave. These proxy records providing evidence of relatively wet conditions at the

LGM support the hypothesis proposed by De Deckker et al. (2020), that water was available during the cold and dry LGM period in Australia, sustaining human populations in inland areas.

115   In summary, there is evidence for widespread cooling over northern, southern and central Australia at the LGM based on a range of proxy records, with the largest cooling inland and at high elevations. In northern Australia, vegetation and fire records suggest drier conditions or possible influences from lower CO_2, while speleothem records may indicate drier conditions. Records from southern and central Australia provide uncertain evidence for hydroclimate change, with some records supporting wetter conditions and others implying drying. Moisture changes may reflect meridional shifts in the
120   westerlies and tropical convergence zone, but evidence for these shifts is also contradictory.

1.2 Climate models simulations of the LGM

Many previous modelling studies have focused on the LGM as this period is one of the main "entry card" experiments for PMIP (Kageyama et al., 2017). However few studies have examined the Southern Hemisphere or the Australian region, as noted above. In this section, we summarise previous LGM modelling studies which focus on the Australian region and major
125   modes of circulation including the Indo-Australian monsoon and the SH mid-latitude westerlies.

Several early studies made use of low-resolution climate models to examine the changes in the Australian monsoon over the late Quaternary (e.g. Wyrwoll and Valdes, 2003; Marshall and Lynch, 2006). In particular, Marshall and Lynch (2006) employed the FOAM model to simulate time-slices including the LGM and found that there was an overall drying over northern Australia at the LGM, with a slight increase during monsoon onset offset by drying during the monsoon peak
130   and retreat. More recently, Yan et al. (2018) examined the Australian monsoon in PMIP3 simulations and found decreased annual and winter precipitation over northern Australia with increases in the early summer (November to December) due to enhanced moisture convergence. This study examines the changes in northern Australian temperature, precipitation and atmospheric circulation in a larger ensemble of models including five models from the latest CMIP6-PMIP4 generation.

The behaviour of the SH westerlies at the LGM is a major area of research with relevance for southern Australian
135   climate. Previous modelling studies using coupled atmosphere-ocean models (PMIP2 and 3) and atmosphere-only models (PMIP1) show ambiguous results regarding the latitudinal positions of the SH mid-latitude westerlies during the LGM. For example, Sime et al. (2013) found strengthening and southward shifts in the maximum 850 hPa SH westerlies based on PMIP2 simulations with an atmosphere-only model (HadAM3). Similarly, a poleward shift in SH surface westerlies was indicated by Kitoh et al. (2001) from an AOGCM used in PMIP1 (MRI-CGCM1 model). However, disagreements are found
140   between different models, with shifts equatorward (Kim et al., 2003) and no latitudinal change (Otto-Bliesner et al., 2006; Rojas et al., 2009) in SH westerlies also observed from PMIP model simulations. This disagreement across model simulations is consistent with a more recent study (Chavaillaz et al., 2013) using the more recent PMIP3 and CMIP5 models, suggesting no agreement was reached between models regarding the latitudinal changes in SH westerlies during the LGM. Rojas (2013) suggested that differences in response may be related to the coupling between atmosphere, ocean and sea ice in

145 the models. Shifts in SH westerlies and the influences on southern and central Australian climate in an ensemble of CMIP5-PMIP3 and CMIP6-PMIP4 models are investigated in this study.

Utilising LGM simulations from an ensemble of CMIP6-PMIP4 and CMIP5-PMIP3 models, this study provides a summary of changes in temperature, precipitation and winds over the Australian region, including both multi-model mean changes and evaluation of model spread or agreement. The drivers of precipitation changes are explored, with reference to 150 changes in regional temperature and circulation patterns. Evidence for changes in the summer monsoon and the mid-latitude westerlies are also examined. The model simulations are compared with proxy reconstructions of temperature and precipitation or moisture balance to determine the extent of model-proxy agreement.

In this paper, the data and methods are described in Section 2, Section 3.1 presents temperature results from models, while wind and precipitation changes at the LGM relative to PI are shown in Section 3.2 and 3.3, respectively. Relationships 155 between climate variables, such as SH mid-latitude westerly winds and precipitation changes at the LGM in JJA season, and the correlations between seasonal temperature and precipitation patterns are evaluated in Section 3.3.2 as drivers of precipitation change. Section 4 discusses the limitations and consistencies between relevant proxy records and modelling studies with our model results, followed by the conclusion in Section 4.4.

2 Data and methods

160 **2.1 Model datasets**

This study makes use of PMIP Phase 3 (PMIP3, Braconnot et al., 2012) model simulations which were included in the Coupled Model Intercomparison Project Phase 5 (CMIP5, Taylor et al., 2012), and PMIP Phase 4 (PMIP4, Kageyama et al., 2018) simulations which were included in CMIP Phase 6 (CMIP6, Eyring et al., 2016). Datasets from eight CMIP5 models and five CMIP6 models that were included in PMIP3 and PMIP4 were analysed, based on data availability via the Earth 165 System Grid Federation (ESGF, the set of models is therefore smaller than Kageyama et al. (2021), who made use of some models only available in PMIP databases). See Table 1 for list of models with LGM simulations included in this study. Monthly surface temperature (ts), surface air temperature (tas), precipitation (pr), evapotranspiration (evspsbl) and 850 hPa wind (ua and va at 850 hPa) data from each model for a model pre-industrial control ('piControl') and LGM ('lgm') simulations were analysed. These variables were chosen to characterise the main features of LGM climate in the region and 170 to facilitate comparison with proxy records of LGM temperature and hydroclimate. All data was re-gridded using first-order conservative remapping onto a $1.5° \times 1.5°$ longitude-latitude grid. Both zonal (u) and meridional (v) components of the wind were analysed, at 850 hPa except for CMIP6 INM-CM4-8 model, which only provided only near-surface (10 m) wind data for LGM simulations. PMIP3/CMIP5 and PMIP4/CMIP6 models shown in Table 1 are referred to as CMIP5 and CMIP6 models hereafter for simplification.

175

Table 1: List of models with LGM data on NCI analysed in this study. The length of simulation years for the LGM run for each model is from Table 1 in Brown et al. (2020). The ice-sheet reconstructions are from Kageyama et al. (2021).

Model	PMIP/CMIP gen.	Lgm run length (years)	Ice-sheet reconstruction	Reference
AWI-ESM-1-1-LR	PMIP4 (CMIP6)	100	ICE-6G_C	Sidorenko et al. (2015), Lohmann et al. (2020)
CCSM4	PMIP3 (CMIP5)	101	PMIP3	Brady et al. (2013)
CESM2-WACCM-FV2	PMIP4 (CMIP6)	500	ICE-6G_C	Zhu et al. (2021)
CNRM-CM5	PMIP3 (CMIP5)	200	PMIP3	Voldoire et al. (2013)
FGOALS-g2	PMIP3 (CMIP5)	100	PMIP3	Zheng and Yu (2013)
GISS-E2-R	PMIP3 (CMIP5)	100	PMIP3	Ullman et al. (2014)
INM-CM4-8	PMIP4 (CMIP6)	200	ICE-6G_C	Volodin et al. (2018)
IPSL-CM5A-LR	PMIP3 (CMIP5)	200	PMIP3	Dufresne et al. (2013)
MIROC-ES2L	PMIP4 (CMIP6)	100	ICE-6G_C	Ohgaito et al. (2021), Hajima et al. (2020)
MIROC-ESM	PMIP3 (CMIP5)	100	PMIP3	Sueyoshi et al. (2013)
MPI-ESM-P	PMIP3 (CMIP5)	100	PMIP3	Adloff et al. (2018)
MPI-ESM1-2-LR	PMIP4 (CMIP6)	500	ICE-6G_C	Mauritsen et al. (2019)
MRI-CGCM3	PMIP3 (CMIP5)	100	PMIP3	Yukimoto et al. (2015)

The models in CMIP6 include some modifications and improvements relative to the older CMIP5 generation (Eyring et al., 2016). There are also some minor differences in the LGM experiment boundary conditions for the CMIP5 (PMIP3) and CMIP6 (PMIP4) experiments. Compared to PMIP3 experiments, new and updated boundary conditions were included in PMIP4 (as shown in Table 2), enabling the systematic analysis of the vegetation and dust forcing effects.

Furthermore, the PMIP4 protocol highlighted the specification of ice sheets, with three distinct ice sheet reconstructions available, allowing assessments of the impacts from uncertainties in ice-sheet reconstructions or boundary conditions (Kageyama et al., 2017). The PMIP3 models used PMIP3 ice-sheet configurations and the five PMIP4 models used in this study are all prescribed using the "ICE-6G_C" ice-sheet reconstruction (see Table 1). The differences between the two LGM
215 ice-sheet reconstructions are discussed in Kageyama et al. (2017). Only CMIP6 AWI-ESM-1-1-LR model is using dynamic vegetation (https://wcrp-cmip.github.io/CMIP6_CVs/docs/CMIP6_source_id.html). The different LGM land fractions configured in each model can be seen in Supplementary Figure S1 showing the land masks for individual models.

Table 2: Summary of the main forcing or boundary conditions (experimental design) for the LGM simulations in PMIP3 and PMIP4
220 models (PMIP4 from Table 1 in Kageyama et al. (2017); PMIP3 from PMIP3 website: https://pmip3.lsce.ipsl.fr/). Some boundary conditions are set as the same as pre-industrial control (piControl) values.

Forcing or Boundary conditions	PMIP4 LGM value	PMIP3 LGM value
Atmospheric trace gases	CO_2 = 190 ppm CH_4 = 375 ppb N_2O = 200 ppb CFC = 0 O_3 = same as in CMIP6 *piControl*	CO_2 = 185 ppm CH_4 = 350 ppb N_2O = 200 ppb CFC = 0 O_3 = same as in CMIP5 *piControl*
Insolation	eccentricity: 0.018994 obliquity: 22.949° perihelion – 180° = 114.42°	eccentricity: 0.018994 obliquity: 22.949° perihelion – 180° = 114.42°
Ice sheets (components of model modified to represent influence of LGM ice sheet)	coastlines bathymetry ice-sheet extent altitude rivers	land-sea mask land surface elevation ocean bathymetry
Vegetation	Unless a model includes dynamic vegetation or interactive dust, the vegetation should be prescribed to be the same as in the DECK and historical runs (CMIP6 *piControl*)	as in *piControl*
Dust	as in *piControl* or *lgm* (three options)	as in *piControl*

2.2 Run Length and Control Simulation

The LGM simulations are compared with pre-industrial (PI) climate as the control or baseline, similarly to many previous
studies (e.g. Kageyama et al., 2021). Pre-industrial ("piControl") experiments are simulations with atmospheric composition
and other boundary conditions prescribed and held constant at values representing climate before industrialization, i.e.
reference year 1850 (Eyring et al., 2016). Most climate models used in this study only have 100-year length of LGM
simulation based on the number of years of data available on the ESGF (refer to Table 1). According to the PMIP protocols,
the models need to spin-up to equilibrium before uploading the data to ESGF (see Kageyama et al. (2017) for details of the
spin-up protocol). At least 100-year data from the equilibrium part of the simulation is required to store on the ESGF
(Kageyama et al., 2017). In this research, the first 100 years of output on the ESGF for each model was selected and
averaged in order to capture the average climatology for each model simulation and to represent the mean state of PI and
LGM climate conditions.

2.3 Classification of Australian Regions

Different regions of Australia experience different climate regimes in the present day, and are likely to respond differently to
LGM climate forcing. Each region also experiences greater seasonal precipitation at a different time of year, with the north
receiving most precipitation in austral summer (DJF season) and the south in austral winter (JJA season). Austral summer is
the period when the Indo-Australian summer monsoon is most active, bringing precipitation to Northern Australia and
nearby SH Maritime Continent areas. In austral winter, the SH westerlies shift equatorward, bringing rainfall to the Southern
Australian region. We therefore divide Australia into three main regions in order to examine the LGM climate response in
detail at seasonal time scales.

Shown in Figure 1, the Australian region is defined in this research bounded by longitudes from 110°E to 160°E,
latitudes from 0 to 45°S. The Northern Australasia domain in the spatial plots is defined longitudes from 110°E to 160° E,
and latitudes from 0 to 20°S (including New Guinea and parts of Indonesia); the Southern Australia domain is defined by
longitudes from 110°E to 160°E, and latitudes from 20°S to 45°S. Lastly, the Central Australian domain is shown in the
spatial plots bounded by 20°S to 35°S and 120°E to 145°E.

3 Results

3.1 Surface air temperature

In this section, the changes in surface air temperature (tas) in the LGM model simulations are evaluated in comparison with
PI simulations. Figure 2 shows the simulated surface air temperature patterns from CMIP5 and CMIP6 model ensembles.
No stippling is seen in Figure 2a and b indicating high model agreements in the ensembles. Despite some differences

between the CMIP6 and CMIP5 model simulations in LGM temperature over Australia (Figure 2c), we combine the five models from CMIP6 and the eight models from CMIP5 together into a large ensemble of thirteen models, for assessing the multi-model mean (MMM) change in temperature patterns at the LGM in this section.

255
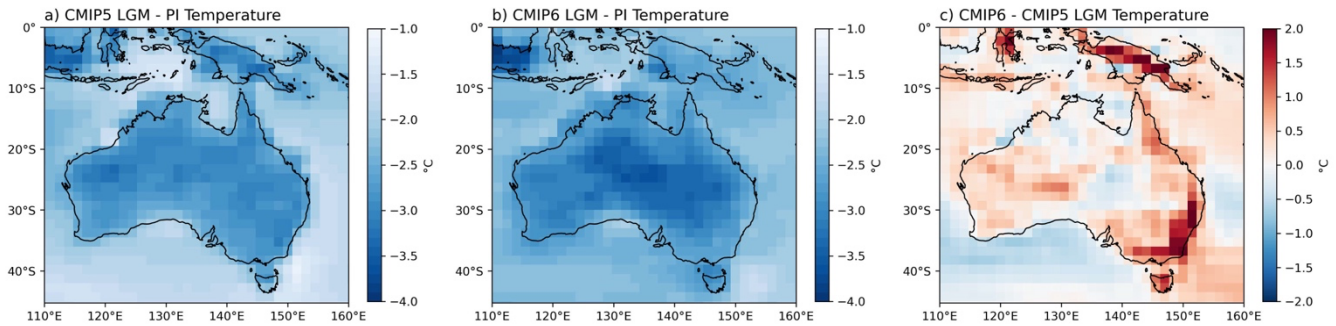
Figure 2: (a) LGM – PI mean annual surface air temperature (in °C) simulated by the ensemble of CMIP5 models, (b) LGM – PI mean annual surface temperature anomaly (in °C) simulated by CMIP6 models, (c) difference between the CMIP6 and CMIP5 LGM ensembles (in °C) over Australian region. Stippling indicates areas where less than 70% of ensemble members agree on the sign of the anomaly.

260

To explore the extent of model agreement for LGM surface air temperatures, Figure 3 shows the annual mean LGM - PI surface air temperature changes over Australia in individual models. All models agree on the sign of temperature change over the Australian region, with mean annual cooling during the LGM compared to PI. The cooling patterns are overall similar across most models, with more cooling over land than ocean. The MMM annual cooling averaged over Australian land areas (using modern coastlines) is -2.9 °C. Those models with greater cooling over the Australian region also tend to have greater global cooling (see Figure 5a and d). We note the much larger cooling in CMIP6 CESM2-WACCM-FV2 model is due to higher climate sensitivity of this model (Zhu et al., 2022), as seen in Figure 5d.

270

275
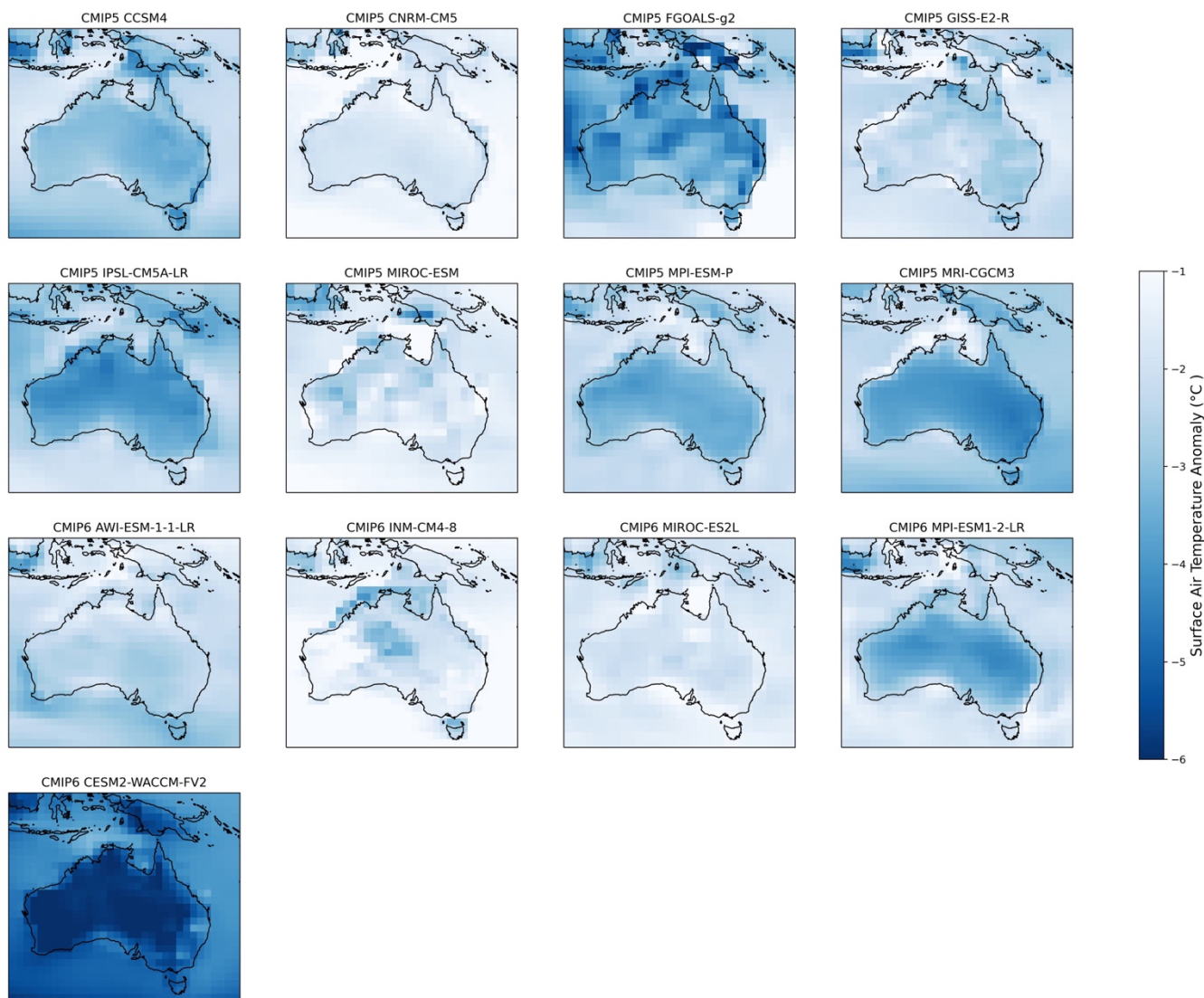
Figure 3: LGM - PI mean annual surface air temperature anomaly (°C) simulated by individual CMIP5 and CMIP6 models over Australian region.

280

      The MMM seasonal variations in surface air temperature changes at the LGM over Australia are shown in Figure 4. The austral winter JJA season shows the strongest land average cooling (-3.1 °C, refer to Figure 5c) at the LGM, particularly along the modern coastlines in both the Northern and Southern Australian regions. LGM cooling is generally larger over land than the surrounding ocean in all seasons, with the exposed Sahul shelf area showing enhanced cooling in all seasons

285   except SON, when there is model disagreement over the sign of the temperature anomaly over Sahul (see Figure 4d).
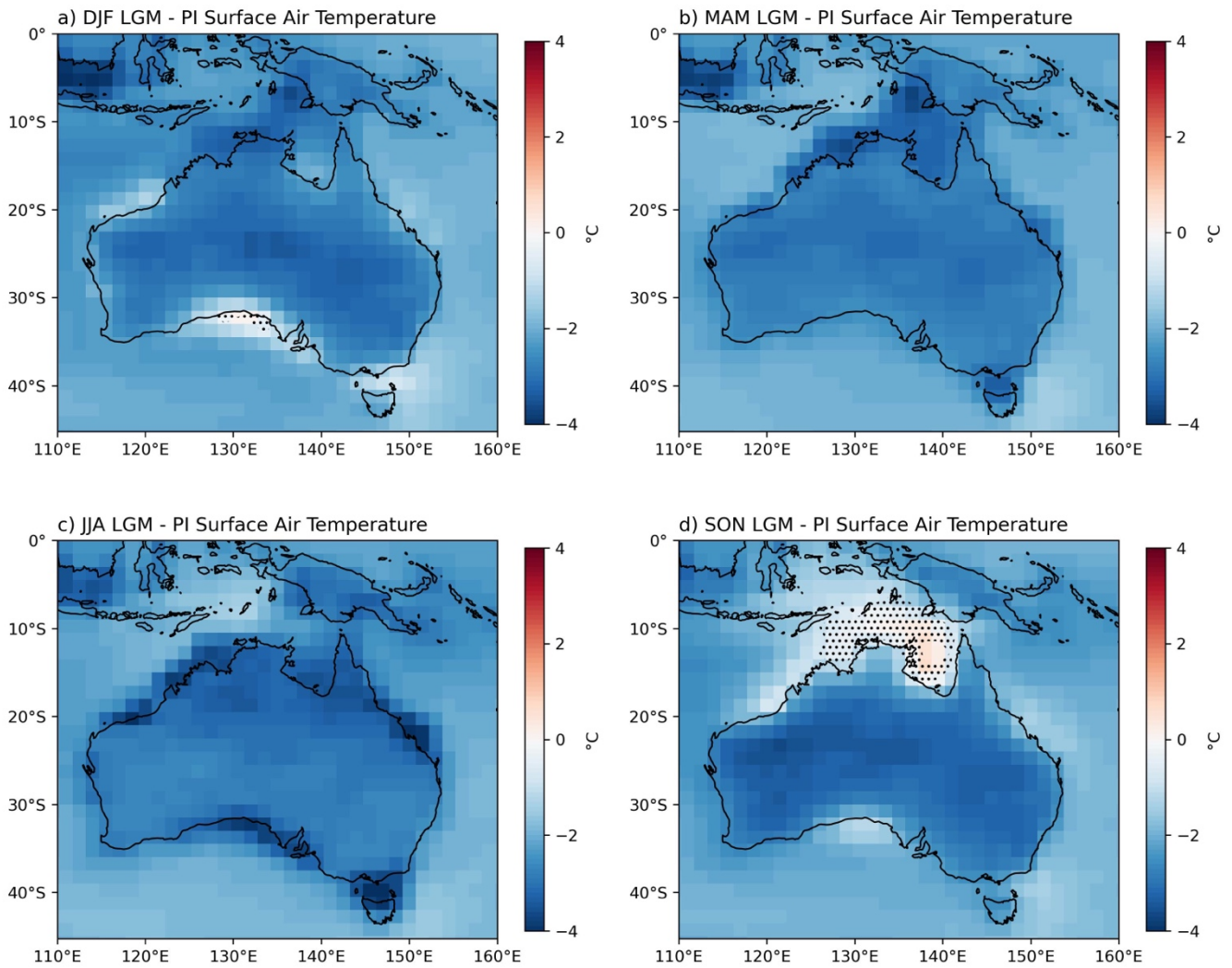
Figure 4: MMM seasonal anomalies for LGM - PI surface air temperatures (°C) simulated by the ensemble of CMIP5 and CMIP6 models for (a) DJF, (b) MAM, (c) JJA and (d) SON seasons over Australian region. Stippling indicates areas where less than 70% of ensemble members agree on the sign of the anomaly.
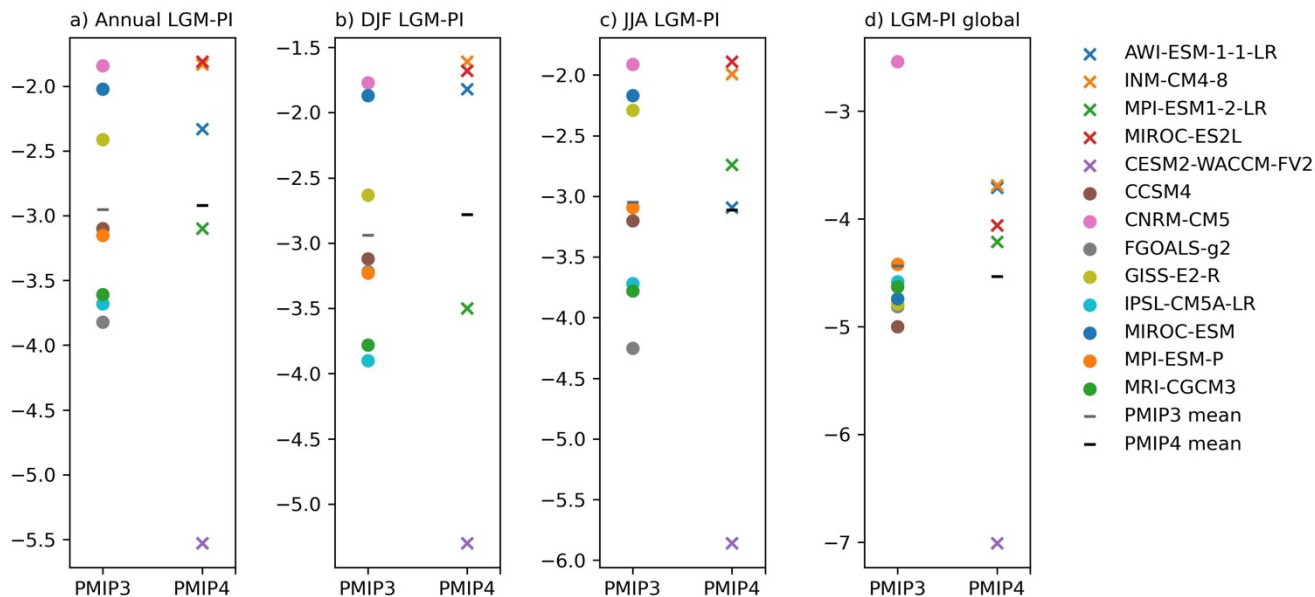
Figure 5: LGM – PI surface air temperature (tas) anomalies (°C) for (a) annual mean, (b) DJF, (c) JJA seasons over Australia (land areas within domain 0-45°S, 110°E-160°E), and (d) global annual mean surface air temperature anomalies (°C) for each CMIP5 and CMIP6 model and the multi-model mean (MMM).

3.2 Winds

This section explores the LGM - PI 850 hPa wind patterns and associated circulation changes from CMIP5/CMIP6 models over the Australian region. MMM seasonal anomalies for LGM - PI 850 hPa zonal winds and wind divergence over Australia are shown in Figure 6 (MMM excludes CMIP6 INM-CM4-8 model, with only 10 m near-surface winds available). We first consider changes over the tropical Northern Australasia domain and then focus on the temperate Southern Australia domain.

In austral summer (DJF) in the modern climate, the Indo-Australian summer monsoon is most active, with north-westerly winds and onshore moisture transport. In the LGM simulations there is a strengthening of the westerly component of the monsoon flow over Northern Australia during DJF (Figure 6a). There are regions of increased wind divergence (orange colors in Figure 6) over the Sahul shelf and parts of the expanded LGM coastline of northwest Australia, with regions of convergence or weakened divergence over adjacent ocean areas. A similar pattern of enhanced onshore westerly flow and wind convergence upstream of the Sahul shelf is seen in austral spring (SON, Figure 6d). Strengthened divergence and offshore flow is seen over this region in MAM (Figure 6c).

In austral winter (JJA) in the modern climate, the SH mid-latitude westerly winds shift northwards, allowing extratropical weather systems to influence Southern Australia. In the LGM simulations, the MMM change in JJA winds (Figure 6c) shows a weakening of the westerlies to the south of around 35°S with little change over Southern Australian land areas, with the exception of a small increase in the westerly winds and wind convergence over the south-west part of this

domain. Individual model simulation results are discussed next to assess the extent of model agreement in JJA season wind changes.
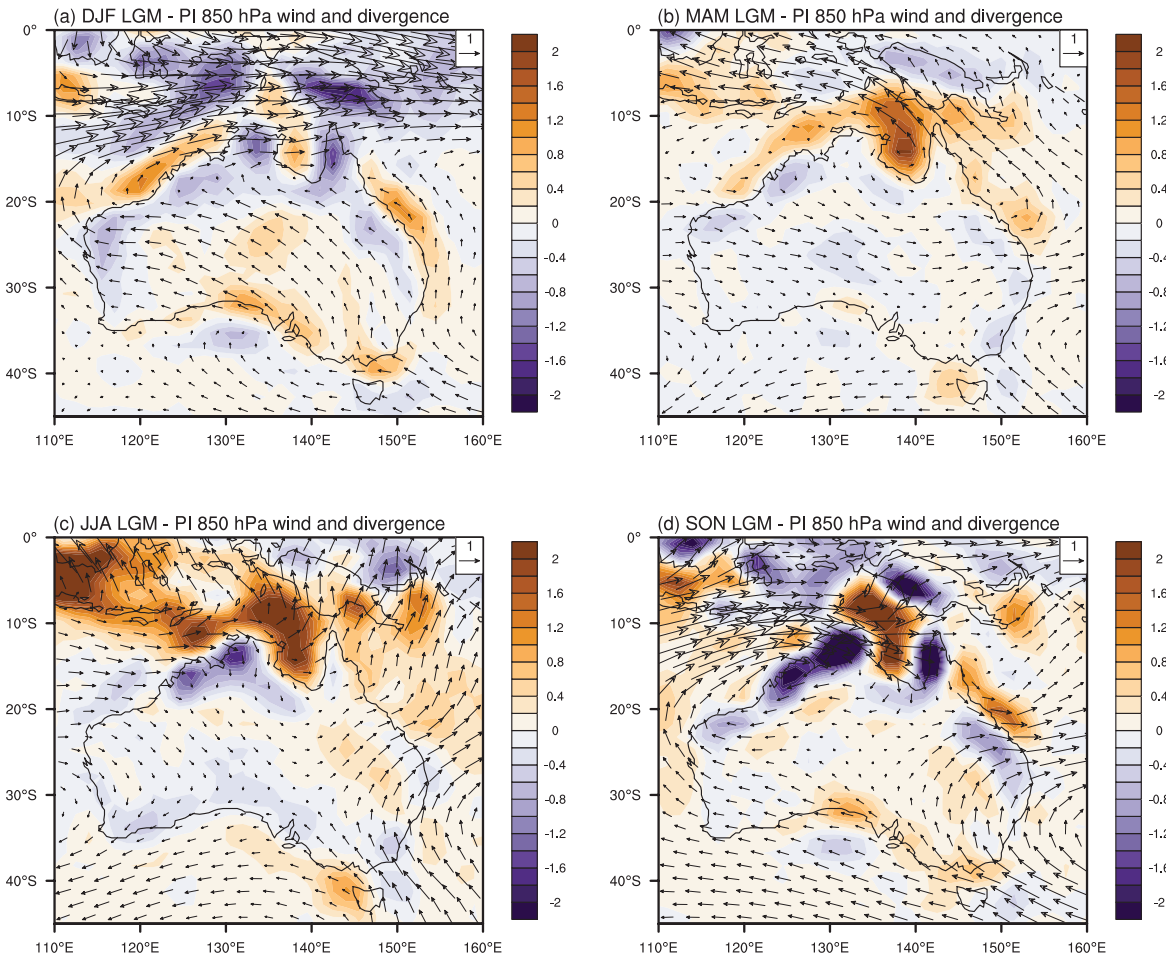
Figure 6: Seasonal average multi-model mean change (lgm – piControl) in 850 hPa winds (m/s) and wind divergence (1 x 10^{-6}/s). Wind change is shown as vectors and wind divergence change is shown as colored contours. MMM excludes INM-CM4-8 model which provided only near-surface winds.

We next investigate the meridional displacement of the SH mid-latitude westerly winds at the LGM, in comparison with previous studies (see Section 1.2), as these winds play an important role in the climate of Southern Australia (e.g. Hope et al., 2010). The LGM change in JJA winds for individual models is shown in Figure 7, with the change in the zonal component of the wind indicated as color shading. It is evident that there is large model disagreement over changes in the mid-latitude westerlies in JJA season in the Australian region. Some models show weakening and other models show

330 strengthening in the region to the south of Australia, with a slight weakening of the MMM westerly wind south of around 35°S as discussed above (see Figure 6).
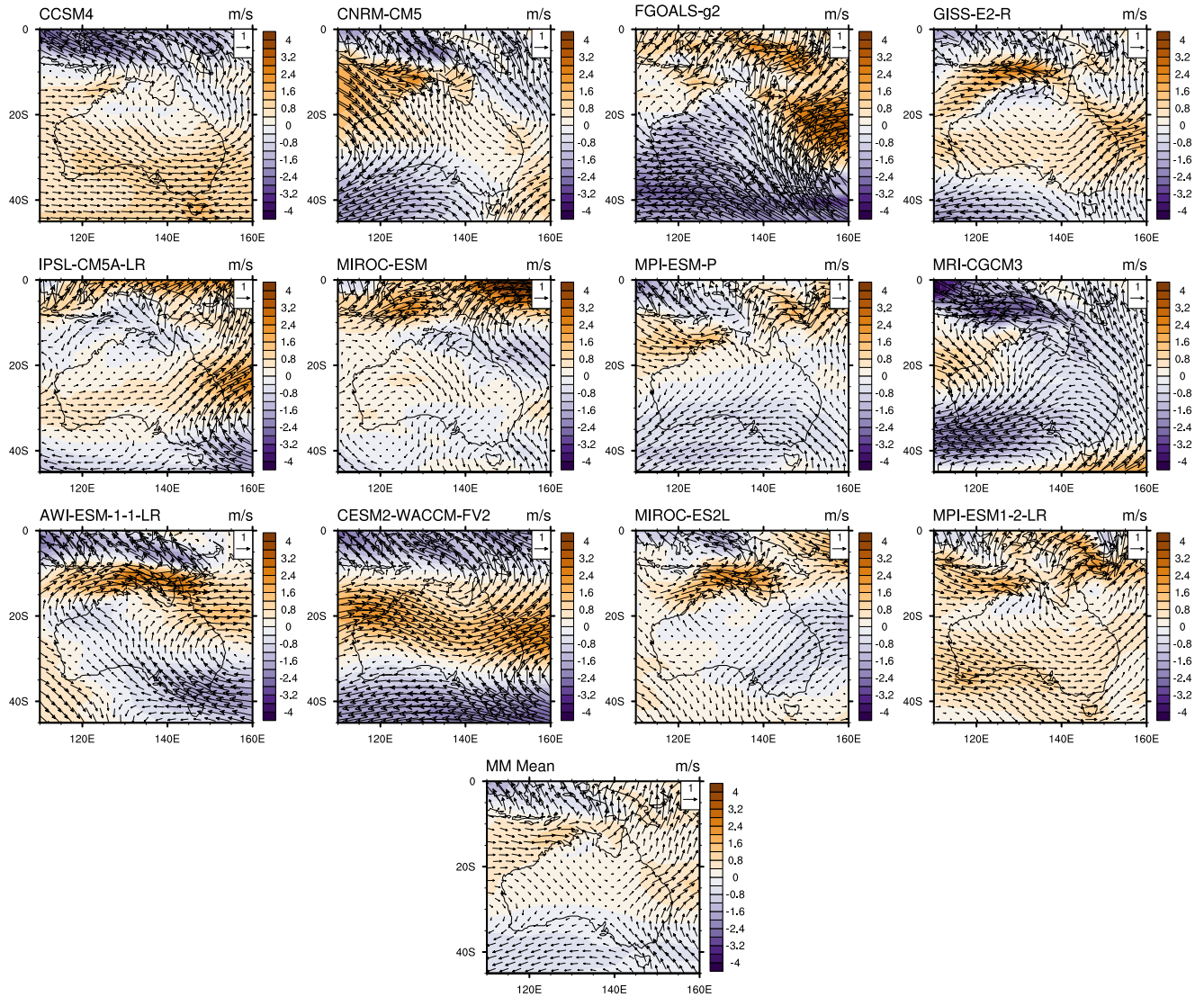
Figure 7: Change in JJA 850 hPa winds (lgm – piControl) for each model and multi-model mean over the Australian domains. Wind
335 change is shown as vectors and zonal (westerly) wind change is shown as colored contours (m/s).

To further investigate shifts in the position of SH westerly winds or changes in their intensity, the zonal-mean zonal wind is plotted over the SH tropics and midlatitudes. Figure 8 shows the zonal-mean 850 hPa zonal winds in JJA over SH (0-

70ºS). The majority of models do not show clear evidence of latitudinal changes for maximum mid-latitude zonal wind speed at the LGM compared to PI, with some disagreements between models (see Figure 8). There is a weak equatorward shift in maximum zonal wind speed seen in IPSL-CM5A-LR and MIROC-ESM models. However, there also seems to be opposite poleward shifts of the maximum zonal winds in CCSM4, FGOALS-g2 and MRI-CGCM3 models. Most models except CCSM4 and MRI-CGCM3 models show overall weakening of SH mid-latitude westerlies at the LGM compared to PI.
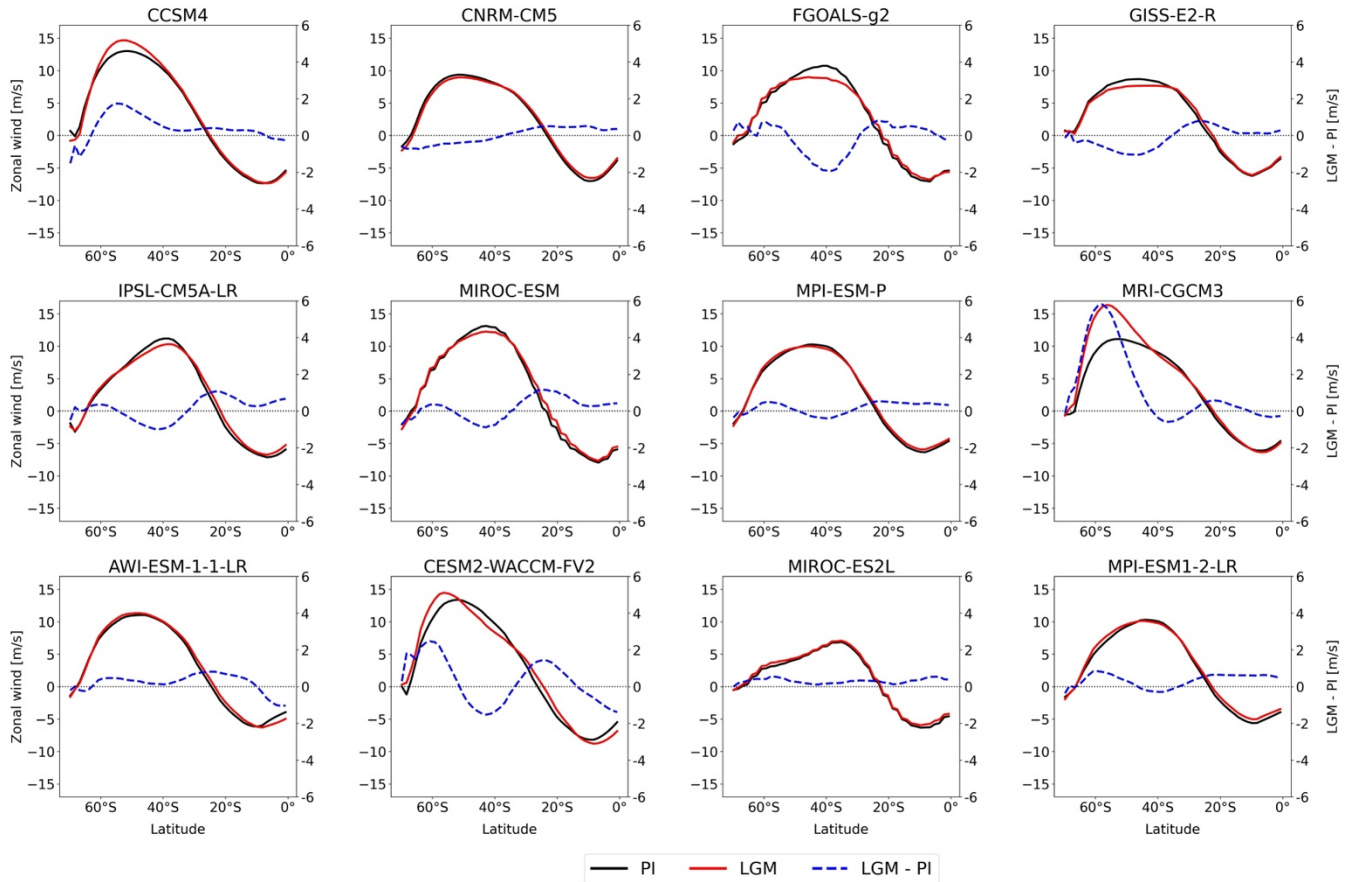
Figure 8: JJA Zonal-mean zonal wind (m/s) at 850 hPa simulated by individual CMIP5 and CMIP6 models (except INM-CM4-8 model which provided only near-surface winds) for SH (0 to 70ºS). PI in black colour and LGM in red colour, blue dashed line is LGM anomalies (LGM - PI). The LGM - PI zonal wind anomaly (m/s) for each model is displayed on a secondary y-axis. Zonal mean is calculated over all longitudes.

3.3 Precipitation

As noted in Section 3.2, in the present-day climate, regional precipitation variations over Australia are associated with seasonal variations in atmospheric circulation. Austral summer (DJF season) is the period when the Indo-Australian summer monsoon is most active, bringing precipitation to northern Australia and nearby Maritime Continent areas. In austral winter (JJA season), the SH westerlies shift equatorward, bringing precipitation to Southern Australia. This section examines the LGM changes in precipitation and moisture balance over the Australian region relative to PI with a focus on seasonal anomalies. The model agreement is also considered.

The LGM - PI annual average precipitation anomalies over Australia for each model are shown in Figure 9. It is evident that the largest model precipitation anomalies occur over Northern Australasia, due to the higher absolute precipitation totals in the tropics. Some models (e.g. GISS-E2-R and INM-CM4-8) simulate increased annual average precipitation over the Sahul shelf region whereas most of the other models show drier conditions. Most models agree on an annual mean decreased precipitation at the LGM averaged over the Australia mainland (see Table 3), however, regional increases in precipitation are also simulated by most models, indicating that thermodynamic reductions in LGM precipitation due to cooling may be offset by dynamical increases at regional scales. Individual model precipitation changes in the DJF and JJA seasons are shown in Supplementary Figures S2 and S3, also displaying model disagreement over tropical regions in DJF but widespread drying in most models in JJA.
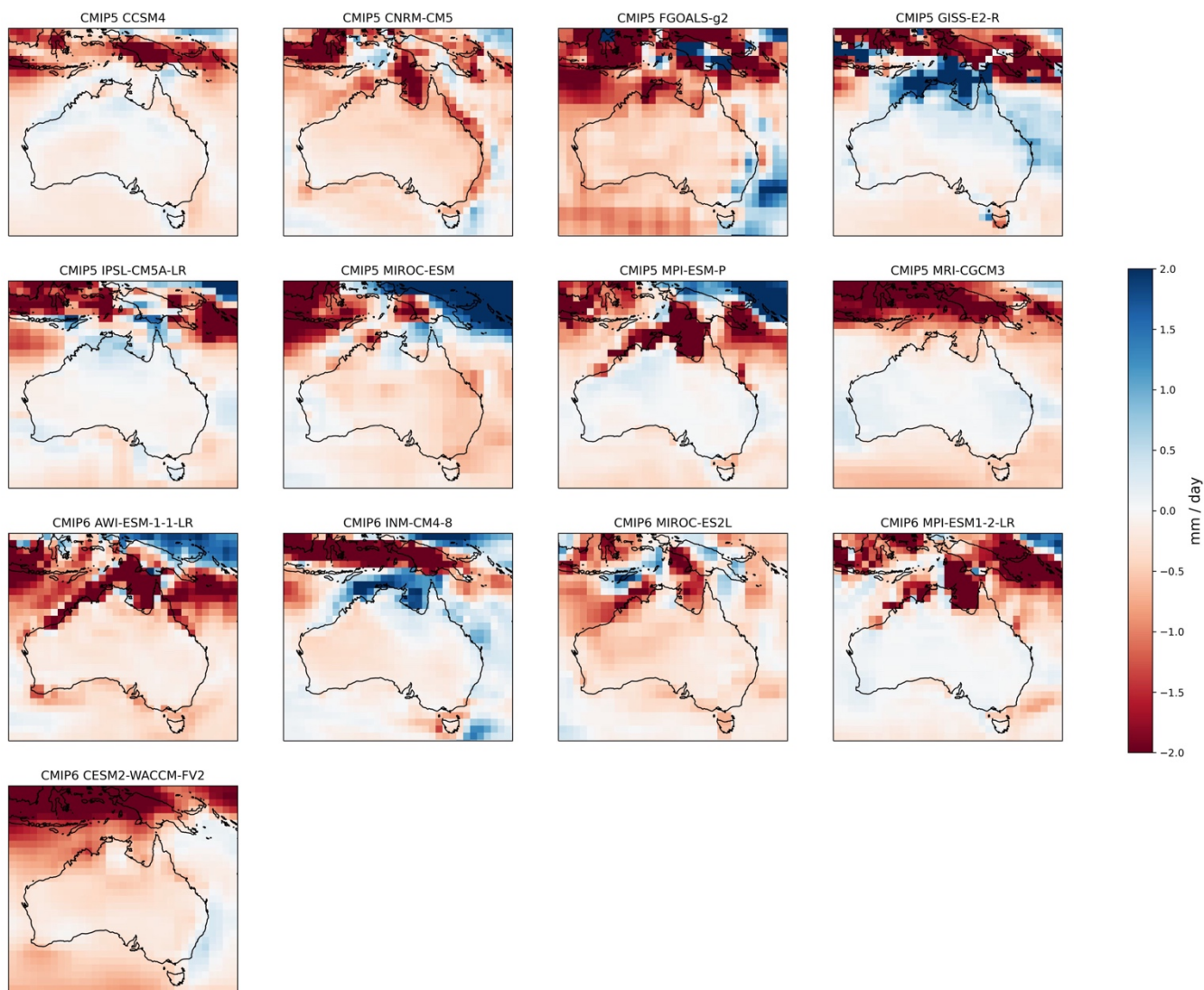
Figure 9: LGM – PI mean annual precipitation anomaly (mm/day) simulated by individual CMIP5 and CMIP6 models over the Australian domains.

MMM seasonal precipitation anomalies from the combined CMIP5 and CMIP6 model ensemble at the LGM over Australia are shown in Figure 10 and seasonal precipitation changes over specific domains are summarised in Table 3. Stippling denotes regions where less than 70% of ensemble members agree on the sign of the anomaly. In austral summer (DJF) season, an increase in precipitation can be seen over parts of Northern Australasia, particularly the central northern Australian region, while other regions become drier (Figure 10a). Most parts of Australia become drier in MAM, with the strongest drying over the Sahul shelf and Maritime Continent, indicating an earlier monsoon retreat (Figure 10b).

Austral winter (JJA) season shows the strongest area-average land drying (-0.59 mm/day) over Australia (0-45°S, 110°E-160°E) during the LGM (Figure 10c). There is a strong precipitation reduction over northern Australia and the Maritime Continent in JJA, consistent with previous analysis of PMIP3 LGM simulations (Yan et al., 2018). The south-western corner of Australia shows an average increase in precipitation in JJA but with low model agreement (Figure 10c). There is a strong increase in precipitation in SON, with high model agreement, over the exposed Sahul shelf and central northern Australia (Figure 10d), as well as along the east coast. This is also consistent with Yan et al. (2018), who identified increased Australian monsoon precipitation in early austral summer (November-December) in PMIP3 LGM simulations.
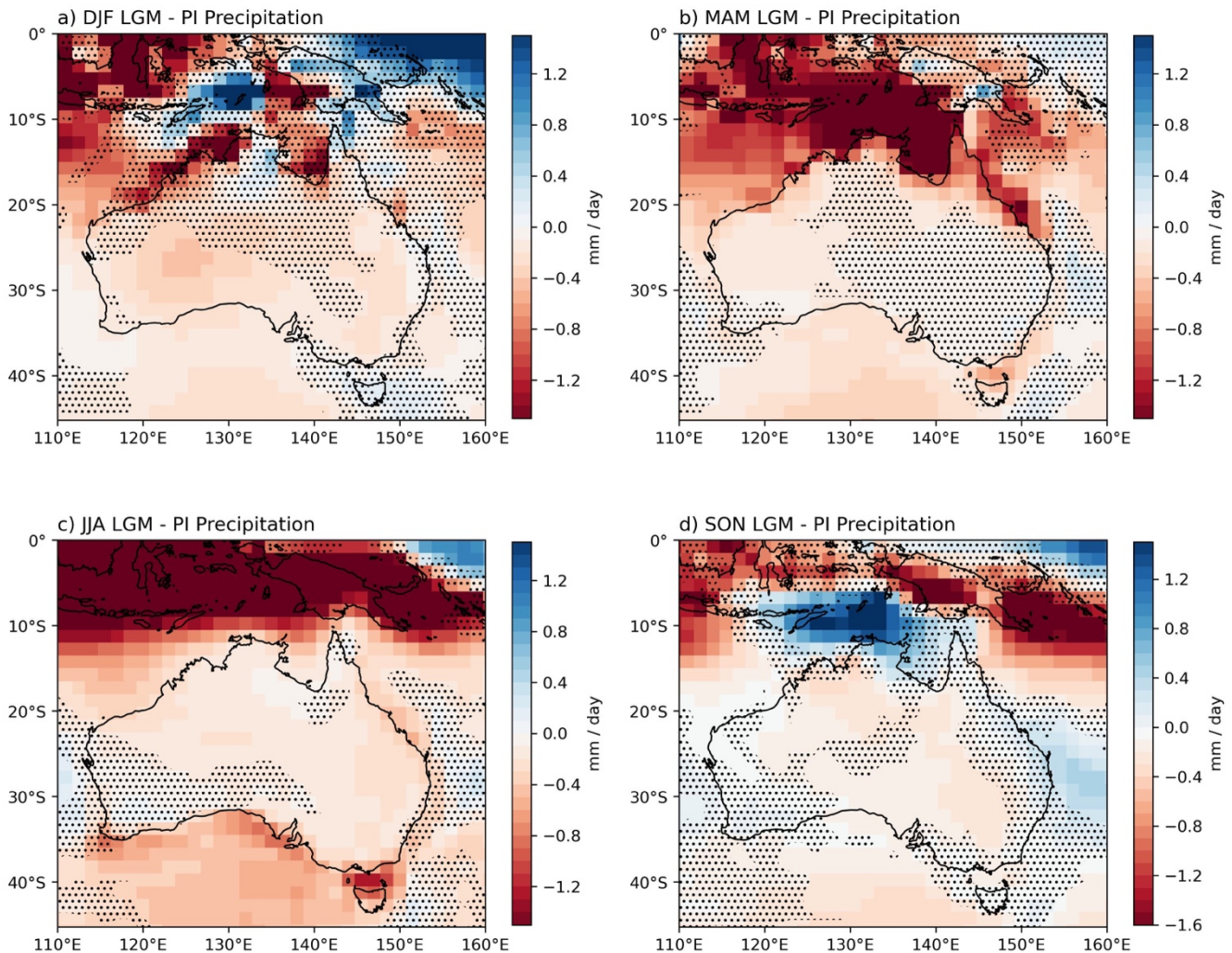
Figure 10: MMM seasonal anomalies for LGM – PI precipitation (mm/day) simulated by the ensemble of CMIP5 and CMIP6 models for (a) DJF, (b) MAM, (c) JJA and (d) SON seasons over Australian region. Stippling indicates areas where less than 70% of ensemble members agree on the sign of the anomaly.

3.3.1 Precipitation minus evapotranspiration (P-E)

As some proxy records provide information about available moisture or effective precipitation changes at the LGM relative to PI, instead of direct evidence for precipitation changes (e.g. Petherick et al., 2013; Sniderman et al., 2019; Fitzsimmons et al., 2012), we also examine changes in the moisture balance or P-E (precipitation minus evapotranspiration) in the LGM simulations. Cooler conditions at the LGM may lead to reduced evaporation and hence a positive P-E despite reduced precipitation (e.g. Scheff et al., 2017; Kageyama et al., 2021).

Annual mean LGM precipitation and evapotranspiration changes over the Australian regions are shown in Figure 11a and b while net precipitation (P-E) is shown in Figure 11c (seasonal mean evapotranspiration changes are shown in Supplementary Figure S4). There is an annual mean reduction in precipitation during the LGM across the Australian mainland, New Guinea and parts of the Maritime Continent, with an annual average land precipitation change of -0.3 mm/day (based on PI land mask, so excluding coastal areas which are land in the LGM only). The strong precipitation reductions simulated in the expanded land areas in the Northern Australasia region and also the exposed Bass Strait region are associated with decreased evaporation rates at the LGM, so that overall increased LGM P-E was simulated (Figure 11). Changes in both precipitation and P-E averaged over different land domains are given in Table 3.
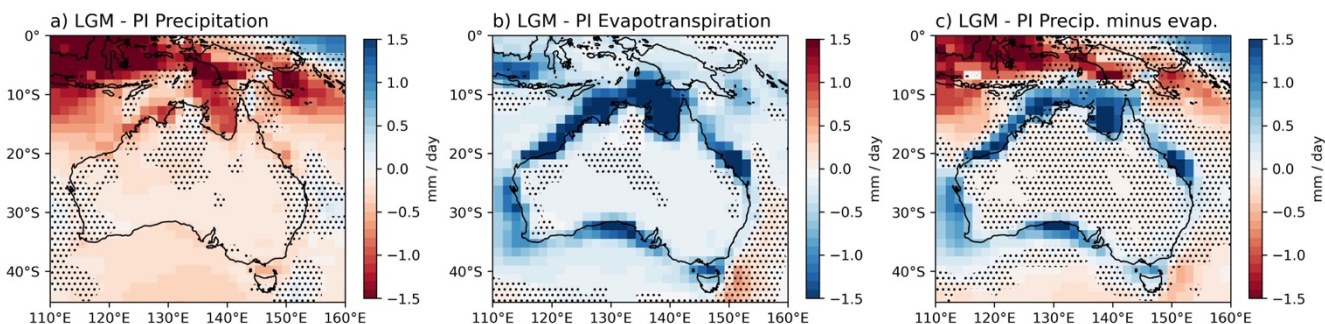
Figure 11: LGM – PI mean annual (a) precipitation (b) evapotranspiration and (b) P-E (in mm/day) simulated by the ensemble of CMIP5 and CMIP6 models over Australian region. Stippling indicates areas where less than 70% of ensemble members agree on the sign of the anomaly.

Figure 12 shows the LGM seasonal variations in net precipitation (P-E) over Australia, which can be compared with the seasonal changes in precipitation shown in Figure 10. In comparison to the variable precipitation pattern at the LGM (Figure 10), the P-E pattern (Figure 12) provides more seasonally consistent spatial changes over Australia during the LGM with the largest increase in P-E over the expanded land areas at the LGM. It is also important to note that model disagreement over the sign of the P-E change is large due to the small magnitude of the changes inland from coastal areas.
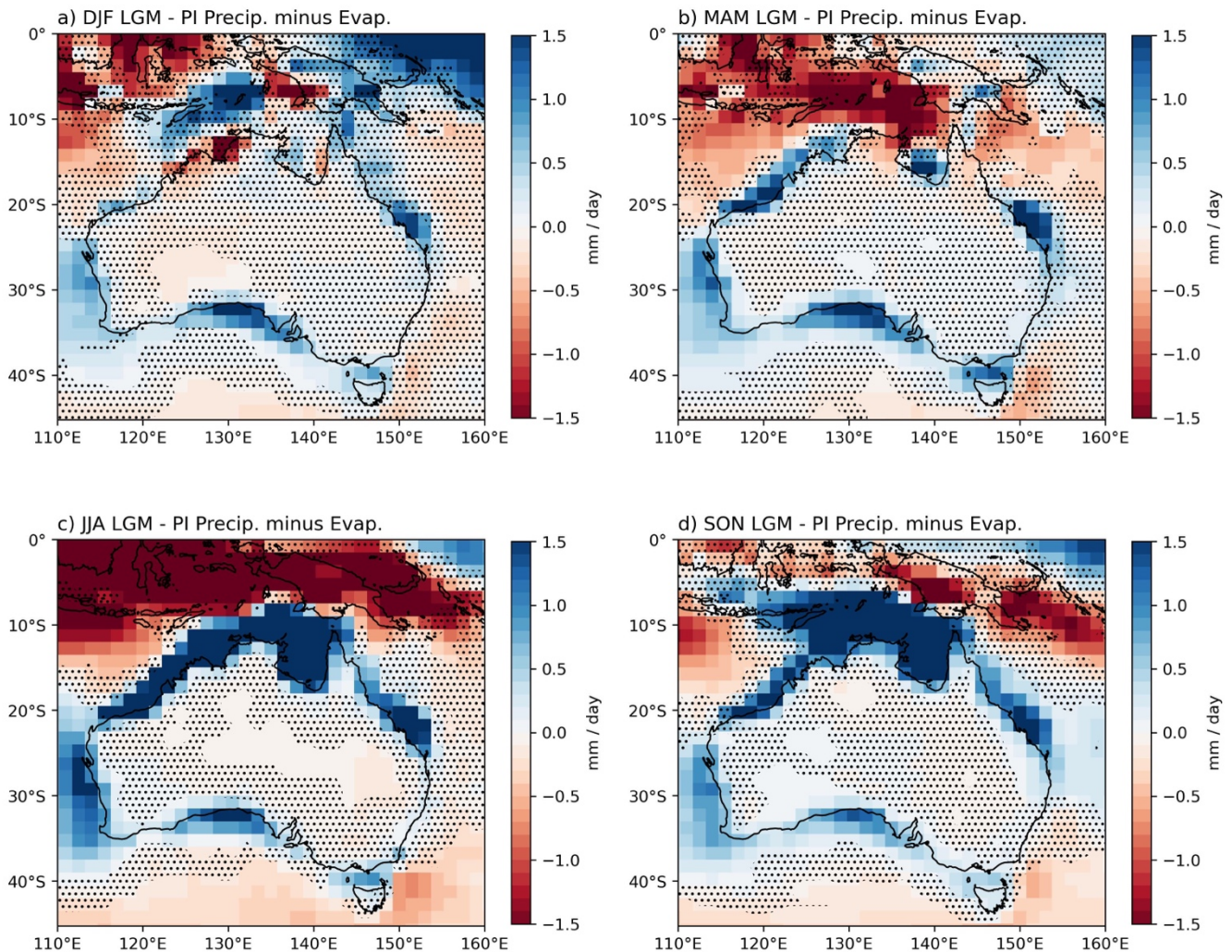
Figure 12: MMM seasonal anomalies for LGM – PI precipitation-evapotranspiration (P-E, mm/day) simulated by the ensemble of CMIP5 and CMIP6 models for (a) DJF, (b) MAM, (c) JJA and (d) SON seasons over Australian region. This can be compared with MMM seasonal precipitation shown in Figure 10 and MMM seasonal evapotranspiration shown in Supplementary Figure S4. Stippling indicates areas where less than 70% of ensemble members agree on the sign of the anomaly.

Table 3 shows the average land precipitation and P-E changes at the LGM in individual models over Northern Australasia in DJF and Southern Australia in JJA and the annual mean anomalies over the mainland Australian area south of 10°S, excluding the Maritime Continent. The Australian mainland region experienced an increase in P-E simulated in all models, with a MMM P-E increase of 0.14 mm/day (Table 3). Individual model simulations of annual average LGM P-E changes are shown in Supplementary Figure S5.

In the Northern Australasia domain, most models show consistent DJF drier conditions in both average LGM precipitation and P-E changes, although large model disagreements occur (see DJF P-E changes in individual models in

Supplementary Figure S6). All models except GISS-E2-R simulated more positive P-E anomalies compared to the corresponding LGM precipitation change. In the Southern Australia region, all models agree on reduced JJA area-average precipitation (see individual model simulations in Supplementary Figure S3) and positive P-E anomalies at the LGM, with the exception of FGOALS-g2 model which has a very small negative JJA P-E anomaly (-0.05 mm/day) (Table 3). Mean P-E changes at the LGM in JJA season for each model over the Australian domain are shown in Supplementary Figure S7. Overall, it is evident that the LGM changes in P-E are less negative (DJF) or positive (JJA and annual average) compared with negative precipitation changes for the MMM and many of the individual models.

Table 3: Average land precipitation and P-E LGM anomalies (mm/day) over Northern Australasia (0-20°S, 110°E-160°E) in DJF season. JJA land averages over Southern Australia (20°S-45°S, 110°E-160°E). Annual mean land average changes for modern Australia mainland (10°S-45°S, 110°E-160°E, excluding Maritime Continent) for each CMIP5 and CMIP6 model and MMM. Land is defined by PI land mask.

Model name	DJF average over Northern Australasia land (mm/day)		JJA average over Southern Australia land (mm/day)		Annual average over modern Australia mainland (mm/day)	
	Precipitation	P - E	Precipitation	P - E	Precipitation	P - E
AWI-ESM-1-1-LR	-0.85	-0.64	-0.25	0.06	-0.38	0.00
CCSM4	-0.48	-0.24	-0.20	0.03	-0.06	0.18
CESM2-WACCM-FV2	-1.88	-1.47	-0.29	0.01	-0.30	0.16
CNRM-CM5	-0.63	-0.12	-0.15	0.19	-0.38	0.10
FGOALS-g2	-0.58	-0.14	-0.70	-0.05	-0.44	0.04
GISS-E2-R	1.02	0.70	-0.14	0.06	0.18	0.31
INM-CM4-8	-0.19	0.18	-0.07	0.21	-0.06	0.22
IPSL-CM5A-LR	1.10	1.17	-0.19	0.10	0.04	0.28
MIROC-ES2L	-0.85	-0.39	-0.19	0.11	-0.37	0.05
MIROC-ESM	0.53	0.74	-0.26	0.10	-0.27	0.11
MPI-ESM-P	-0.83	-0.20	-0.03	0.10	-0.12	0.05
MPI-ESM1-2-LR	-0.61	-0.25	-0.03	0.11	-0.08	0.08
MRI-CGCM3	-1.23	-0.86	-0.04	0.25	0.00	0.30
MMM	-0.42	-0.12	-0.20	0.10	-0.17	0.14

3.3.2 Drivers of precipitation change

LGM cooling is likely to lead to overall drier conditions due to the thermodynamic response (a colder atmosphere holds less moisture), as seen in the annual mean MMM change (Figure 2). However, the models do not simulate drying over all regions or in all seasons over Australia. For instance, annually wetter conditions are found over the south-west of Australia and parts of the tropics in some models (Figure 9) and regions of increased MMM precipitation are found over the tropics in DJF and SON (Figures 10). While a decomposition of thermodynamic and dynamic components of precipitation change is not included in this study, it is evident that the thermodynamic drying response is dominant over much of the Australian land area in the individual models and the seasonal MMM precipitation changes.

Over the Northern Australasia domain, the seasonal precipitation changes are complex and not clearly linked to temperature changes over either land or ocean. However, changes in temperature gradients between land and ocean may be important in driving circulation change (see Supplementary Figure S8 for annual surface temperature changes over Northern Australia in each model, with different LGM land mask configurations shown in Supplementary Figure S1). The exposure of the Sahul shelf appears to drive changes in moisture transport, with increased onshore westerlies (Figure 6) driving convergence upstream of the LGM coastline, producing increased precipitation to the northwest of Australia over a small region in DJF (Figure 10a) and a larger region in SON (Figure 10d). The disagreement in simulated austral summer precipitation between models (Supplementary Figure S2) can also be linked to different changes in circulation in the models (not shown). Offshore wind anomalies and increased wind divergence in MAM and JJA produces widespread drying over the entire Northern Australasia region. Further analysis of moisture convergence fields is required to confirm this mechanism, but it is broadly consistent with the findings of Yan et al. (2018) based on PMIP3 LGM simulations.

LGM precipitation changes over Southern Australia appear to be dominated by thermodynamic drying, with additional contributions from dynamical processes including shifts in the position or intensity of the SH mid-latitude westerlies. While area average precipitation changes over the Southern Australia domain are negative in JJA, the majority of models simulate increased precipitation over the south-west corner of Southern Australia (see Supplementary Figure S3).

This region is also climatically distinct in the modern climate, experiencing higher winter rainfall than surrounding areas, with a recent strong drying trend (Hope et al. 2010).

We explored the relationship between the JJA LGM change in precipitation averaged over south-west Australia (30ºS-35ºS, 115ºE-120ºE) and the change in strength of the westerly winds over the same latitude range, but with a wider longitude range for the entire Southern Australian region (110°E-155°E). The corresponding scatter plot is shown in Supplementary Figure S9. The Pearson correlation coefficient between the two variables is $r = 0.52$, and the corresponding p-value is 0.081, indicating that the correlation is not significant at the 95% confidence level. Sime et al. (2013) found that there is no clear relationship between the displacements of westerlies and enhanced precipitation at the LGM based on PMIP models, which is consistent with our findings. However, the positive anomalies in the south-west indicate a dynamical driver of precipitation increase is stronger than thermodynamic drying in this region.

4 Discussion and Conclusions

This study has evaluated the temperature, precipitation and wind changes over the Australian region at the LGM compared with pre-industrial conditions from CMIP5 and CMIP6 model simulations. We now summarise the key finding from the model simulations and briefly compare these with published proxy records of LGM temperature, precipitation and atmospheric circulation from this region, introduced in Section 1.

4.1 Temperature

The LGM ensemble of thirteen CMIP5 and CMIP6 models simulates a global annual cooling of surface air temperature of -4.5 ºC compared to PI conditions, within the range proposed in other modelling studies (e.g. Annan et al., 2022; Tierney et al., 2020a). Regionally, the models simulate cooling of annual surface air temperatures in the range of -1.8 ºC to -5.5 ºC (MMM = -2.9 ºC) in the Australian domain (0-45°S, 110°E-160°E), with larger cooling over land and particularly over coastal regions with expanded land area at the LGM. On seasonal time scales, cooling is slightly larger in MAM and JJA over this region. Our model results for temperature change generally agree well with available proxy records and previous modelling studies although there are some LGM proxy records that imply greater LGM cooling than the models. For example, Miller et al. (1997) and Hope (2009) reconstructed greater cooling over land than was simulated by the models, with Miller et al. (1997) finding cooling of 9 ºC in inland Australia and Hope (2009) finding cooling of 4-6 ºC in the New Guinea highlands. This may be due to uncertainties in the proxy reconstruction. Alternatively, the models may not be simulating the extent of cooling over land in the LGM simulations. In the case of proxy records over high topography (e.g. Hope, 2009), the models also may not have resolved the details of the topography and associated cooling.

4.2 Precipitation

The models simulate an overall reduced precipitation over the Australian region, with negative annual average anomalies in the majority of models and the MMM. Seasonal MMM precipitation anomalies (Figure 10) indicate widespread, slightly lower precipitation than today, except for slightly higher precipitation during DJF, in the north-eastern central Northern Australia, northern Cape York, and all of Tasmania except the west coast; during JJA in SW western Australia; and during SON in the subtropical eastern margin of the continent. Examination of the P-E patterns (Figure 12) shows most of the continent experienced reduced precipitation but positive P-E anomalies, implying that most regions at the LGM would have experienced little change in moisture availability, or slightly wetter conditions, particularly on seasonal time scales.

Some paleoclimate proxies (e.g. Fitzsimmons et al., 2013; Petherick et al., 2013; Cadd et al., 2018; Rowe et al., 2021) have been interpreted as indicating substantially lower LGM moisture availability, which is not consistent with the changes in P-E from the PMIP/CMIP simulations analysed in this study. On the other hand, studies of paleo-river channels near the Murray-Darling Basin indicate that relatively high fluvial discharge, and thus moisture availability, were maintained at the LGM (e.g. Cohen et al., 2015; Kemp et al., 2017; Treble et al., 2017; Hesse et al., 2018). The contradiction between

some proxy reconstructions and model simulations may reflect the fact that vegetation-based hydroclimate reconstructions have not taken into account the effects of low atmospheric CO_2 on plant growth, which is increasingly recognised as a factor that should not be ignored (Prentice et al., 2017; Scheff et al., 2017; Sniderman et al., 2019). Moreover, it is increasingly suspected (e.g. Scheff et al., 2017; Roderick et al., 2015) that greater LGM dustiness and dune-mobilisation are secondary effects from reduced plant productivity, via landscape destabilisation. Alternatively, the large model disagreement suggests that at least some models are not realistically simulating the LGM hydroclimate response in this region. The reasons for this are beyond the scope of the present study, but likely reflect biases in model convection, land surface interactions or other relevant processes.

4.3 Winds

Similar to many previous studies, we did not find a consistent equatorward or poleward shift in the SH mid-latitude westerly winds at the LGM over the Australian longitude range or a wider SH zonal average (not shown) based on the available CMIP5 and CMIP6 model simulations. Over the south-west corner of Southern Australia, increased LGM precipitation in austral winter (JJA) was more likely in models with strengthened SH westerlies over the surrounding domain, although the correlation was not significant. However, we did not identify a consistent shift in maximum SH mid-latitude zonal winds in the LGM simulations

4.4 Conclusions

This research presents an initial evaluation and analysis of climate conditions (temperature, precipitation, wind) over the Australian domain (including adjacent regions of Indonesia and New Guinea) at the LGM using an ensemble of eight CMIP5 and five CMIP6 models with available PMIP LGM simulations. The results offer insights into regional Australian climate variations during the LGM, and the inter-connections between climate variables in different seasons. Our model results show widespread cooling in the annual mean and all seasons, with a magnitude that is generally consistent with available proxy records except in central Australia and high elevations in New Guinea, where models show less cooling than proxy records.

The models disagree on changes in precipitation over Northern Australasia in austral summer, with a complex multi-model mean pattern of precipitation change. The lack of model agreement indicates that each model responds differently to the specified changes in boundary conditions at the LGM, producing different changes in circulation and therefore different dynamical components of the precipitation response. This implies that caution is required when comparing proxy records with simulations from a single model or small group of models in this tropical region. Uncertainty in both model simulations and the interpretation of proxy records of hydroclimate limits quantitative model-proxy comparisons.

In Southern Australia, the changes in precipitation indicate widespread drying over land in all seasons, except for the southwest of the continent. The changes in the position or intensity of the SH westerlies are not consistent between

555 models, again suggesting that caution is required when comparing simulations from a single model with proxy records from this region. Given the large changes in global and regional temperature in the LGM simulations, with similar patterns of cooling in all models, it is noteworthy that the models do not simulate a consistent shift in this important component of the regional circulation, suggesting that shifts in the position of the westerlies cannot be assumed as a simple response to large-scale climate cooling (or warming).

560   Further analysis is required to better understand the divergent model responses to LGM boundary conditions in both the tropics and mid-latitudes in the Australian region. This analysis may also provide guidance for understanding model responses in a future warming climate. Comparison with well constrained proxy records of past hydroclimate changes would also provide a useful target for identifying more realistic model simulations. Such comparison will need to consider the moisture balance rather than focusing only on precipitation, and will need to account for sensitivity of some proxies to 565 changes in CO_2 levels.

Code and data availability

The CMIP5 and CMIP6 model data used in this study are available from the Earth System Grid Federation.

Supplement

The Supplement related to this article is available online at:

570 **Author contributions**

YD and JRB designed the study. YD carried out the data analysis and led the writing of the manuscript. JRB and JMKS provided comments on the results and contributed to the writing of the manuscript.

Competing interests

The authors declare that they have no conflict of interest.

575 **Acknowledgments**

Josephine R. Brown and Yanxuan Du acknowledge support from the Australian Research Council Centre of Excellence for Climate Extremes (CE170100023). We acknowledge the World Climate Research Programme, which, through its Working Group on Coupled Modelling, coordinated and promoted CMIP6. We thank the climate modelling groups for producing and making available their model output, the Earth System Grid Federation (ESGF) for archiving the data and providing access,

and the multiple funding agencies who support CMIP6 and ESGF. CMIP5 and CMIP6 model outputs were made available with the assistance of resources from the National Computational Infrastructure (NCI), which is supported by the Australian government.

References

Adloff, M., Reick, C. H., and Claussen, M.: Earth system model simulations show different feedback strengths of the terrestrial carbon cycle under glacial and interglacial conditions, Earth Syst. Dynam., 9, 413–425, https://doi.org/10.5194/esd-9-413- 2018, 2018.

Annan, J. D. and Hargreaves, J. C.: A new global reconstruction of temperature changes at the Last Glacial Maximum, Clim. Past, 9, 367–376, https://doi.org/10.5194/cp-9-367-2013, 2013.

Annan, J. D., Hargreaves, J. C., and Mauritsen, T.: A new global surface temperature reconstruction for the Last Glacial Maximum, Clim. Past, 18, 1883–1896, https://doi.org/10.5194/cp-18-1883-2022, 2022.

Bird, M. I., O'Grady, D., and Ulm, S.: Humans, water, and the colonization of Australia, Proc. Natl. Acad. Sci. U.S.A., 113, 11477-11482, https://doi.org/10.1073/pnas.1608470113, 2016.

Braconnot, P., Harrison, S. P., Kageyama, M., Bartlein, P. J., Masson-Delmotte, V., Abe-Ouchi, A., Otto-Bliesner, B., and Zhao, Y.: Evaluation of climate models using palaeoclimatic data, Nat. Clim. Change, 2, 417-424, https://doi.org/10.1038/nclimate1456, 2012.

Bradshaw, C. J. A., Norman, K., Ulm, S., Williams, A. N., Clarkson, C., Chadœuf, J., Lin, S. C., Jacobs, Z., Roberts, R. G., Bird, M. I., Weyrich, L. S., Haberle, S. G., O'Connor, S., Llamas, B., Cohen, T. J., Friedrich, T., Veth, P., Leavesley, M., and Saltré, F.: Stochastic models support rapid peopling of Late Pleistocene Sahul, Nat. Commun., 12, 2440, https://doi.org/10.1038/s41467-021-21551-3, 2021.

Brady, E. C., Otto-Bliesner, B. L., Kay, J. E., and Rosenbloom, N.: Sensitivity to Glacial Forcing in the CCSM4, J. Climate, 26, 1901–1925, https://doi.org/10.1175/JCLI-D-11-00416.1, 2013.

Brown, J. R., Brierley, C. M., An, S. I., Guarino, M. V., Stevenson, S., Williams, C. J. R., Zhang, Q., Zhao, A., Abe-Ouchi, A., Braconnot, P., Brady, E. C., Chandan, D., D'Agostino, R., Guo, C., LeGrande, A. N., Lohmann, G., Morozova, P. A., Ohgaito, R., O' ishi, R., Otto-Bliesner, B. L., Peltier, W. R., Shi, X., Sime, L., Volodin, E. M., Zhang, Z., and Zheng, W.:

Comparison of past and future simulations of ENSO in CMIP5/PMIP3 and CMIP6/PMIP4 models, Clim. Past, 16, 1777-1805, https://doi.org/10.5194/cp-16-1777-2020, 2020.

615   Byrne, M.: Evidence for multiple refugia at different time scales during Pleistocene climatic oscillations in southern Australia inferred from phylogeography, Quaternary Sci. Rev., 27, 2576-2585, https://doi.org/10.1016/j.quascirev.2008.08.032, 2008.

Cadd, H. R., Tibby, J., Barr, C., Tyler, J., Unger, L., Leng, M. J., Marshall, J. C., McGregor, G., Lewis, R., Arnold, L. J.,
620   Lewis, T., and Baldock, J.: Development of a southern hemisphere subtropical wetland (Welsby Lagoon, south-east Queensland, Australia) through the last glacial cycle, Quaternary Sci. Rev., 202, 53-65, https://doi.org/10.1016/j.quascirev.2018.09.010, 2018.

Cadd, H., Petherick, L., Tyler, J., Herbert, A., Cohen, T., Sniderman, K., Barrows, T. T., Fulop, R. T., Knight, J., Kershaw,
625   A. P., Colhoun, E. A., and Harris, M.: A continental perspective on the timing of environmental change during the last glacial stage in Australia, Quaternary Res., 102, 5-23, https://doi.org/10.1017/qua.2021.16, 2021.

Chadwick, R., Boutle, I., and Martin, G.: Spatial patterns of precipitation change in CMIP5: Why the rich do not get richer in the tropics, J. Climate, 26, 3803-3822, https://doi.org/10.1175/JCLI-D-12-00543.1, 2013.

630
Chavaillaz, Y., Codron, F., and Kageyama, M.: Southern westerlies in LGM and future (RCP4.5) climates, Clim. Past, 9, 517-524, https://doi.org/10.5194/cp-9-517-2013, 2013.

Clark, P. U., Dyke, A. S., Shakun, J. D., Carlson, A. E., Clark, J., Wohlfarth, B., Mitrovica, J. X., Hostetler, S. W., and
635   McCabe, A. M.: The Last Glacial Maximum, Science, 325, 710–714, https://doi.org/10.1126/science.1172873, 2009.

Clarkson, C., Jacobs, Z., Marwick, B., Fullagar, R., Wallis, L., Smith, M., Roberts, R. G., Hayes, E., Lowe, K., Carah, X., Florin, S. A., McNeil, J., Cox, D., Arnold, L. J., Hua, Q., Huntley, J., Brand, H. E. A., Manne, T., Fairbairn, A., Shulmeister, J., Lyle, L., Salinas, M., Page, M., Connell, K., Park, G., Norman, K., Murphy, T., and Pardoe, C.: Human occupation of
640   northern Australia by 65,000 years ago, Nature, 547, 306, https://doi.org/10.1038/nature22968, 2017.

Cohen, T.J., John, D. J., Luke, A. G., Joshua, R. L., Gerald, C. N., Jan-Hendrik, M., Brian, G. J., and David, M. P.: Hydrological transformation coincided with megafaunal extinction in central Australia, Geology, 43, 195–198, https://doi.org/10.1130/G36346.1, 2015.

645

Danabasoglu, G., Lamarque, J.-F., Bacmeister, J., Bailey, D. A., DuVivier, A. K., Edwards, J., Emmons, L. K., Fasullo, J., Garcia, R., Gettelman, A., Hannay, C., Holland, M. M., Large, W. G., Lauritzen, P. H., Lawrence, D. M., Lenaerts, J. T. M., Lindsay, K., Lipscomb, W. H., Mills, M. J., Neale, R., Oleson, K. W., Otto-Bliesner, B., Phillips, A. S., Sacks, W., Tilmes, S., van Kampenhout, L., Vertenstein, M., Bertini, A., Dennis, J., Deser, C., Fischer, C., Fox-Kemper, B., Kay, J. E.,

650   Kinnison, D., Kushner, P. J., Larson, V. E., Long, M. C., Mickelson, S., Moore, J. K., Nienhouse, E., Polvani, L., Rasch, P. J., and Strand, W. G.: The Community Earth System Model Version 2 (CESM2), J. Adv. Model. Earth Syst., 12, e2019MS001916, https://doi.org/10.1029/2019MS001916, 2020.

Denniston, R. F., Wyrwoll, K. H., Asmerom, Y., Polyak, V. J., Humphreys, W. F., Cugley, J., Woods, D., LaPointe, Z.,

655   Peota, J., and Greaves, E.: North Atlantic forcing of millennial-scale Indo-Australian monsoon dynamics during the Last Glacial period, Quaternary Sci. Rev., 72, 159-168, https://doi.org/10.1016/j.quascirev.2013.04.012, 2013.

De Deckker, P., Moros, M., Perner, K., Blanz, T., Wacker, L., Schneider, R., Barrows, T. T., O' Loingsign, T., and Jansen, E.: Climatic evolution in the Australian region over the last 94 ka - spanning human occupancy -, and unveiling the Last

660   Glacial Maximum, Quaternary Sci. Rev., 249, https://doi.org/10.1016/j.quascirev.2020.106593, 2020.

DiNezio, P. N., and Tierney, J. E.: The effect of sea level on glacial Indo-Pacific climate, Nat. Geosci., 6, 485-491, https://doi.org/10.1038/NGEO1823, 2013.

665   Dufresne, J. L., Foujols, M. A., Denvil, S., Caubel, A., Marti, O., Aumont, O., Balkanski, Y., Bekki, S., Bellenger, H., Benshila, R., Bony, S., Bopp, L., Braconnot, P., Brockmann, P., Cadule, P., Cheruy, F., Codron, F., Cozic, A., Cugnet, D., de, Noblet, N., Duvel, J. P., Ethé, C., Fairhead, L., Fichefet, T., Flavoni, S., Friedlingstein, P., Grandpeix, J. Y., Guez, L., Guilyardi, E., Hauglustaine, D., Hourdin, F., Idelkadi, A., Ghattas, J., Joussaume, S., Kageyama, M., Krinner, G., Labetoulle, S., Lahellec, A., Lefebvre, M. P., Lefevre, F., Levy, C., Li, Z. X., Lloyd, J., Lott, F., Madec, G., Mancip, M.,

670   Marchand, M., Masson, S., Meurdesoif, Y., Mignot, J., Musat, I., Parouty, S., Polcher, J., Rio, C., Schulz, M., Swingedouw, D., Szopa, S., Talandier, C., Terray, P., Viovy, N., and Vuichard, N.: Climate change projections using the IPSL-CM5 Earth System Model: from CMIP3 to CMIP5, Clim. Dynam., 40, 2123–2165, https://doi.org/10.1007/s00382-012-1636-1, 2013.

Ehlers, J., and Gibbard, P. L.: The extent and chronology of Cenozoic Global Glaciation, Quat. Int., 164-165, 6-20,

675   https://doi.org/10.1016/j.quaint.2006.10.008, 2007.

Eyring, V., Bony, S., Meehl, G. A., Senior, C. A., Stevens, B., Stouffer, R. J., and Taylor, K. E.: Overview of the Coupled Model Intercomparison Project Phase 6 (CMIP6) experimental design and organization, Geosci. Model Dev., 9, 1937–1958, https://doi.org/10.5194/gmd-9-1937-2016, 2016.

680

Fitzsimmons, K. E., Cohen, T. J., Hesse, P. P., Jansen, J., Nanson, G. C., May, J.-H., Barrows, T. T., Haberlah, D., Hilgers, A., Kelly, T., Larsen, J., Lomax, J., and Treble, P.: Late Quaternary palaeoenvironmental change in the Australian drylands, Quaternary Sci. Rev., 74, 78-96, https://doi.org/10.1016/j.quascirev.2012.09.007, 2013.

685   Fitzsimmons, K. E., Miller, G. H., Spooner, N. A., and Magee, J. W.: Aridity in the monsoon zone as indicated by desert dune formation in the Gregory Lakes basin, northwestern Australia, Aust. J. Earth Sci., 59, 469-478, https://doi.org/10.1080/08120099.2012.686171, 2012.

Hajima, T., Watanabe, M., Yamamoto, A., Tatebe, H., Noguchi, M. A., Abe, M., Ohgaito, R., Ito, A., Yamazaki, D.,
690   Okajima, H., Ito, A., Takata, K., Ogochi, K., Watanabe, S., and Kawamiya, M.: Development of the MIROC-ES2L Earth system model and the evaluation of biogeochemical processes and feedbacks, Geosci. Model Dev., 13, 2197–2244, https://doi.org/10.5194/gmd-13- 2197-2020, 2020.

Hesse, P. P., Williams, R., Ralph, T. J., Frirs, K. A., Larkin, Z. T., Westaway, K. E., and Farebrother, W.: Palaeohydrology
695   of lowland rivers in the Murray-Darling Basin, Australia, Quaternary Sci. Rev., 200, 85-105, https://doi.org/10.1016/j.quascirev.2018.09.035, 2018.

Holden, P. B., Edwards, N. R., Oliver, K. I. C., Lenton, T. M., and Wilkinson, R. D.: A probabilistic calibration of climate sensitivity and terrestrial carbon change in GENIE-1, Clim. Dynam., 35, 785, https://doi.org/10.1007/s00382-009-0630-8,
700   2010.

Hope, G.: Environmental change and fire in the Owen Stanley Ranges, Papua New Guinea, Quaternary Sci. Rev., 28, 2261-2276, https://doi.org/10.1016/j.quascirev.2009.04.012, 2009.

705   Hope, P: The Weather and Climate of Australia at the Last Glacial Maximum, PhD Thesis, University of Melbourne, School of Earth Sciences, 2005.

Hope, P., Timbal, B., and Fawcett, R.: Associations between rainfall variability in the southwest and southeast of Australia and their evolution through time, Int. J. Climatol., 30, 1360-1371, https://doi.org/10.1002/joc.1964, 2010.
710

Hughes, P. D., Gibbard, P. L., and Ehlers, J.: Timing of glaciation during the last glacial cycle: evaluating the concept of a global 'Last Glacial Maximum' (LGM), Earth-Sci Rev., 125, 198–171, https://doi.org/10.1016/j.earscirev.2013.07.003, 2013.

715 Jungclaus, J., Mikolajewicz, U., Kapsch, M.-L., D'Agostino, R., Wieners, K.-H., Giorgetta, M., Reick, C., Esch, M., Bittner, M., Legutke, S., Schupfner, M., Wachsmann, F., Gayler, V., Haak, H., de Vrese, P., Raddatz, T., Mauritsen, T., von Storch, J.-S., Behrens, J., Brovkin, V., Claussen, M., Crueger, T., Fast, I., Fiedler, S., Hagemann, S., Hohenegger, C., Jahns, T., Kloster, S., Kinne, S., Lasslop, G., Kornblueh, L., Marotzke, J., Matei, D., Meraner, K., Modali, K., Müller, W., Nabel, J., Notz, D., Peters, K., Pincus, R., Pohlmann, H., Pongratz, J., Rast, S., Schmidt, H., Schnur, R., Schulzweida, U., Six, K.,
720 Stevens, B., Voigt, A., and Roeckner, E.: MPI-M MPI-ESM1.2-LR model output prepared for CMIP6 PMIP lgm, Version 20190710, Earth System Grid Federation, https://doi.org/10.22033/ESGF/CMIP6.6642, 2019.

Kageyama, M., Albani, S., Braconnot, P., Harrison, S. P., Hopcroft, P. O., Ivanovic, R. F., Lambert, F., Marti, O., Peltier, W. R., Peterschmitt, J.-Y., Roche, D. M., Tarasov, L., Xu Zhang, Brady, E. C., Haywood, A. M., LeGrande, A. N., Lunt, D. J.,
725 Mahowald, N. M., Mikolajewicz, U., and Nisancioglu, K. H.: The PMIP4 contribution to CMIP6 - Part 4: Scientific objectives and experimental design of the PMIP4-CMIP6 Last Glacial Maximum experiments and PMIP4 sensitivity experiments, Geosci. Model Dev., 10, 4035–4055, https://doi.org/10.5194/gmd-10-4035-2017, 2017.

Kageyama, M., Braconnot, P., Harrison, S. P., Haywood, A. M., Jungclaus, J. H., Otto-Bliesner, B. L., Peterschmitt, J.-Y.,
730 Abe-Ouchi, A., Albani, S., Bartlein, P. J., Brierley, C., Crucifix, M., Dolan, A., Fernandez-Donado, L., Fischer, H., Hopcroft, P. O., Ivanovic, R. F., Lambert, F., Lunt, D. J., Mahowald, N. M., Peltier, W. R., Phipps, S. J., Roche, D. M., Schmidt, G. A., Tarasov, L., Valdes, P. J., Zhang, Q., and Zhou, T.: The PMIP4 contribution to CMIP6 – Part 1: Overview and over-arching analysis plan, Geosci. Model Dev., 11, 1033–1057, https://doi.org/10.5194/gmd-11-1033-2018, 2018.

735 Kageyama, M., Harrison, S. P., Kapsch, M.-L., Lofverstrom, M., Lora, J. M., Mikolajewicz, U., Sherriff-Tadano, S., Vadsaria, T., Abe-Ouchi, A., Bouttes, N., Chandan, D., Gregoire, L. J., Ivanovic, R. F., Izumi, K., LeGrande, A. N., Lhardy, F., Lohmann, G., Morozova, P. A., Ohgaito, R., Paul, A., Peltier, W. R., Poulsen, C. J., Quiquet, A., Roche, D. M., Shi, X., Tierney, J. E., Valdes, P. J., Volodin, E., and Zhu, J.: The PMIP4 Last Glacial Maximum experiments: preliminary results and comparison with the PMIP3 simulations, Clim. Past, 17, 1065–1089, https://doi.org/10.5194/cp-17-1065-2021, 2021.
740
Kemp, J., Pietsch, T., Gontz, A., and Olley, J: Lacustrine-fluvial interactions in Australia's Riverine Plains, Quaternar Sci. Rev., 166, 352-362, https://doi.org/10.1016/j.quascirev.2017.02.015, 2017.

Kim, S. J., Flato, G., and Boer, G.: A coupled climate model simulation of the Last Glacial Maximum, Part 2: approach to
745 equilibrium, Clim. Dynam., 20, 635-661, https://doi.org/10.1007/s00382-002-0292-2, 2003.

Kitoh, A., Murakami, S., and Koide, H.: A simulation of the Last Glacial Maximum with a coupled atmosphere-ocean GCM, 28, 2221-2224, https://doi.org/10.1029/2000GL012271, 2001.

750 Kohfeld, K. E., Graham, R. M., de Boer, A. M., Sime, L. C., Wolff, E. W., Le Quéré, C., and Bopp, L.: Southern Hemisphere westerly wind changes during the Last Glacial Maximum: paleo-data synthesis, Quaternary Sci. Rev., 68, 76-95, https://doi.org/10.1016/j.quascirev.2013.01.017, 2013.

Lambeck, K., Rouby, H., Purcell, A., Sun, Y., and Sambridge, M.: Sea level and global ice volumes from the Last Glacial
755 Maximum to the Holocene, Proc. Natl. Acad. Sci. U.S.A., 111, 15296–15303, https://doi.org/10.1073/pnas.1411762111, 2014.

Lamy, F., Gersonde, R., Winckler, G., Esper, O., Jaeschke, A., Kuhn, G., Ullermann, J., Martinez-Garcia, A., Lambert, F., and Kilian, R.: Increased Dust Deposition in the Pacific Southern Ocean During Glacial Periods, Science, 343, 404–407,
760 https://doi.org/10.1126/science.l245424, 2014.

Liu, Z., Lu, Z., Wen, X., Otto-Bliesner, B. L., Timmermann, A., and Cobb, K. M.: Evolution and forcing mechanisms of El Niño over the past 21,000 years, Nature, 515, 550-553, https://doi.org/10.1038/nature13963, 2014.

765 Liu, S., Jiang, D., and Lang, X.: The Weakening and Eastward Movement of ENSO Impacts during the Last Glacial Maximum, J. Climate, 33, 5507-5526, https://doi.org/10.1175/JCLI-D-19-0728.1, 2020.

Marshall, A. G., and Lynch, A. H.: Time-slice analysis of the Australian summer monsoon during the late Quaternary using the Fast Ocean Atmosphere Model, J. Quat. Sci., 21, 789-801, https://doi.org/10.1002/jqs.1063, 2006.
770
Miller, G. H., Magee, J. W., and Jull, A. J. T.: Low-latitude glacial cooling in the Southern Hemisphere from amino-acid racemization in emu eggshells, Nature, 385, 241-244, https://doi.org/10.1038/385241a0, 1997.

Nevill, P. G., Bossinger, G., and Ades, P. K.: Phylogeography of the world's tallest angiosperm, Eucalyptus regnans:
775 evidence for multiple isolated Quaternary refugia, J. Biogeogr., 37, 179-192, https://doi.org/10.1111/j.1365-2699.2009.02193.x, 2010.

Newnham, R. M., Lowe, D. J., Giles, T., and Alloway, B. V.: Vegetation and climate of Auckland, New Zealand, since ca. 32 000 cal. yr ago: Support for an extended LGM, J. Quat. Sci., 22, 517–534, https://doi.org/10.1002/jqs.1137, 2007.
780

Ohgaito, R., Yamamoto, A., Hajima, T., O'ishi, R., Abe, M., Tatebe, H., Abe-Ouchi, A., and Kawamiya, M.: PMIP4 experiments us- ing MIROC-ES2L Earth system model, Geosci. Model Dev., 14, 1195–1217, https://doi.org/10.5194/gmd-14-1195-2021, 2021.

785 Otto-Bliesner, B. L., Brady, E. C., Clauzet, G., Tomas, R., Levis, S., and Kothavala, Z.: Last Glacial Maximum and Holocene Climate in CCSM3, J. Climate, 9, 2526-2544, https://doi.org/10.1175/JCLI3748.1, 2006.

Pepper, M. and Keogh, J. S.: Life in the "dead heart" of Australia: The geohistory of the Australian deserts and its impact on genetic diversity of arid zone lizards, J. Biogeogr., 48, 716-746, https://doi.org/10.1111/jbi.14063, 2021.
790

Petherick, L., Bostock, H., Cohen, T. J., Fitzsimmons, K., Tibby, J., Fletcher, M. S., Moss, P., Reeves, J., Monney, S., Barrows, T., Kemp, J., Jansen, J., Nanson, G., and Dosseto, A.: Climatic records over the past 30 ka from temperate Australia – a synthesis from the Oz-INTIMATE workgroup, Quaternary Sci. Rev., 74, 58-77, https://doi.org/10.1016/j.quascirev.2012.12.012, 2013.
795

Prentice, I. C., Cleator, S. F., Huang, Y. H., Harrison, S. P., and Roulstone, I.: Reconstructing ice-age palaeoclimates: Quantifying low-CO_2 effects on plants, Glob. Planet. Change., 149, 166–176, https://doi.org/10.1016/j.gloplacha.2016.12.012, 2017.

800 Prentice, I. C., Harrison, S. P., and Bartlein, P. J.: Global vegetation and terrestrial carbon cycle changes after the last ice age, New Phytol., 189, 988–998, https://doi.org/10.1111/j.1469-8137.2010.03620.x, 2011.

Prentice, I. C., Villegas-Diaz, R., and Harrison, S. P.: Accounting for atmospheric carbon dioxide variations in pollen-based reconstruction of past hydroclimates, Glob. Planet. Change., 211, https://doi.org/10.1016/j.gloplacha.2022.103790, 2022.
805

Reeves, J. M., Bostock, H. C., Ayliffe, L. K., Barrows, T. T., De Deckker, P., Devriendt, L. S., Dunbar, G. B., Drysdale, R. N., Fitzsimmons, K. E., Gagan, M. K., Griffiths, M. L., Haberle, S. G., Jansen, J. D., Krause, C., Lewis, S., McGregor, H. V., Mooney, S. D., Moss, P., Nanson, G. C., Purcell, A., and van der Kaars, S.: Palaeoenvironmental change in tropical Australasia over the last 30,000 years - a synthesis by the OZ-INTIMATE group, Quaternary Sci. Rev., 74, 97-114,
810 https://doi.org/10.1016/j.quascirev.2012.11.027, 2013a.

Reeves, J. M., Barrows, T. T., Cohen, T. J., Kiem, A. S., Bostock, H. C., Fitzsimmons, K. E., Jansen, J. D., Kemp, J., Krause, C., Petherick, L., and Phipps, S. J.: Climate variability over the last 35,000 years recorded in marine and terrestrial

archives in the Australian region: an OZ-INTIMATE compilation, Quaternary Sci. Rev., 74, 21-34, https://doi.org/10.1016/j.quascirev.2013.01.001, 2013b.

Renoult, M., Annan, J. D., Hargreaves, J. C., Sagoo, N., Flynn, C., Kapsch, M.-L., Li, Q., Lohmann, G., Mikolajewicz, U., Ohgaito, R., Shi, X., Zhang, Q., and Mauritsen, T.: A Bayesian framework for emergent constraints: case studies of climate sensitivity with PMIP, Clim. Past, 16, 1715–1735, https://doi.org/10.5194/cp-16- 1715-2020, 2020.

Roderick, M. L., Farquhar, G. D., and Greve, P.: On the assessment of aridity with changes in atmospheric CO_2, Water Resour. Res., 51, 5450–5463, https://doi.org/10.1002/2015WR017031, 2015.

Rojas, M.: Sensitivity of Southern Hemisphere circulation to LGM and 4 × CO2 climates, Geophys. Res. Lett., 40, 965-970, https://doi.org/10.1002/grl.50195, 2013.

Rojas, M., Moreno, P., Kageyama, M., Crucifix, M., Hewitt, C., Abe-Ouchi, A., Ohgaito, R., Brady, E. C., and Hope, P.: Southern Westerlies during the last glacial maximum in PMIP2 simulations, Clim. Dynam., 32, 525–548, https://doi.org/10.1007/s00382-008-0421-7, 2009.

Rowe, C., Wurster, C., Zwart, C., Brand, M., Hutley, L., Levchenko, V., and Bird, M.: Vegetation over the last glacial maximum at Girraween Lagoon, monsoonal northern Australia, Quaternary Res., 102, 39-52, https://doi.org/10.1017/qua.2020.50, 2021.

Scheff, J., Seager, R., Liu, H., and Coats, S.: Are Glacials Dry? Consequences for Paleoclimatology and for Greenhouse Warming, J. Climate, 30, 6593-6609, https://doi.org/10.1175/JCLI-D-16-0854.1, 2017.

Schneider von Deimling, T., Held, H., Ganopolski, A., and Rahmstorf, S.: Climate sensitivity estimated from ensemble simulations of glacial climate, Clim. Dynam., 27, 149-163, https://doi.org/10.1007/s00382-006-0126-8, 2006.

Seltzer, A. M., Ng, J., Aeschbach, W., Kipfer, R., Kulongoski, J. T., Severinghaus, J. P., and Stute, M.: Widespread six degrees Celsius cooling on land during the Last Glacial Maximum, Nature, 593, 228–232, https://doi.org/10.1038/s41586-021-03467-6, 2021.

Sidorenko, D., Rackow, T., Jung, T., Semmler, T., Barbi, D., Danilov, S., Dethloff, K., Dorn, W., Fieg, K., Goßling, H. F., Handorf, D., Harig, S., Hiller, W., Juricke, S., Losch, M., Schröter, J., Sein, D. V., and Wang, Q.: Towards multi-resolution

global climate modeling with ECHAM6-FESOM, Part I: model formulation and mean climate, Clim. Dynam., 44, 757–780, https://doi.org/10.1007/s00382-014-2290-6, 2015.

850 Sime, L. C., Kohfeld, K. E., Le Quéré, C., Wolff, E. W., de Boer, A. M., Graham, R. M., and Bopp, L.: Southern Hemisphere westerly wind changes during the Last Glacial Maximum: model-data comparison, Quaternary Sci. Rev., 64, 104-120, https://doi.org/10.1016/j.quascirev.2012.12.008, 2013.

Sniderman, J. M. K., Hellstrom, J., Woodhead, J. D., Drysdale, R. N., Bajo, P., Archer, M., and Hatcher, L.: Vegetation and 855 climate change in southwestern Australia during the Last Glacial Maximum, Geophys. Res. Lett., 46, 1709–1720, https://doi.org/10.1029/2018GL080832, 2019.

Sueyoshi, T., Ohgaito, R., Yamamoto, A., Chikamoto, M. O., Hajima, T., Okajima, H., Yoshimori, M., Abe, M., O'ishi, R., Saito, F., Watanabe, S., Kawamiya, M., and Abe-Ouchi, A.: Set-up of the PMIP3 paleoclimate experiments conducted using 860 an Earth system model, MIROC-ESM, Geosci. Model Dev., 6, 819–836, https://doi.org/10.5194/gmd-6-819-2013, 2013.

Taylor, K. E., Stouffer, R. J., and Meehl, G. A.: An Overview of CMIP5 and the Experiment Design, Bull. Amer. Meteor., 93, 485–498, https://doi.org/10.1175/BAMS-D-11-00094.1, 2012.

865 Tierney, J. E., Zhu, J., King, J., Malevich, S. B., Hakim, G. J., and Poulsen, C. J.: Glacial cooling and climate sensitivity revisited, Nature, 584, 569-573, https://doi.org/10.1038/s41586-020-2617-x, 2020a.

Tierney, J. E., Poulsen, C. J., Montanez, I. P., Bhattacharya, T., Feng, R., Ford, H. L., Hönisch, B., Inglis, G. N., Petersen, S. V., Sagoo, N., Tabor, C. R., Thirumalai, K., Zhu, J., Burls, N. J., Foster, G. L., Goddéris, Y., Huber, B. T., Ivany, L. C., 870 Turner, S. K., Lunt, D. J., McElwain, J. C., Mills, B. J. W., Otto-Bliesner, B. L., Ridgwell, A., and Zhang, Y. G.: Past climates inform our future, Science, 370, eaay3701, https://doi.org/10.1126/science.aay3701, 2020b.

Treble, P. C., Baker, A., Ayliffe, L. K., Cohen, T. J., Hellstrom, J. C., Gagan, M. K., Frisia, S., Drysdale, R. N., Griffiths, A. D., and Borsato, A.: Hydroclimate of the Last Glacial Maximum and deglaciation in southern Australia's arid margin 875 interpreted from speleothem records (23–15 ka), Clim. Past, 13, 667-687, https://doi.org/10.5194/cp-13-667-2017, 2017.

Ullman, D. J., LeGrande, A. N., Carlson, A. E., Anslow, F. S., and Licciardi, J. M.: Assessing the impact of Laurentide Ice Sheet topography on glacial climate, Clim. Past, 10, 487–507, https://doi.org/10.5194/cp-10-487-2014, 2014.

880 Ujvari, G., Wegner, W., Klotzli, U., Horschinegg, M., and Hippler, D.: Sr-Nd-Hf Isotopic Analysis of < 10 mg Dust Samples: Implications for Ice Core Dust Source Fingerprinting, Geochem. Geophys., 19, 60–63, https://doi.org/10.1002/2017GC007136, 2018.

Voldoire, A., Sanchez-Gomez, E., Salas y Mélia, D., Decharme, B., Cassou, C., Sénési, S., Valcke, S., Beau, I., Alias, A.
885 Chevallier, M., Déqué, M., Deshayes, J., Douville, H., Fernan- dez, E., Madec, G., Maisonnave , E., Moine, M.-P., Planton, S., Saint-Martin, D., Szopa, S., Tyteca, S., Alkama, R., Bela- mari, S., Braun, A., Coquart, L., and Chauvin, F.: The CNRM-CM5.1 global climate model: description and basic evaluation, Clim. Dynam., 40, 2091–2121, https://doi.org/10.1007/s00382- 011-1259-y, 2013.

890 Volodin, E., Mortikov, E., Kostrykin, S., Galin, V., Lykossov, V., Gritsun, A., Diansky, N., Gusev, A., Iakovlev, N., Shestakova, A., and Emelina, S.: Simulation of the modern climate us- ing the INM-CM48 climate model, Russian Journal of Nu- merical Analysis and Mathematical Modelling, 33, 367–374, https://doi.org/10.1515/rnam-2018-0032, 2018.

Wang, T., Wang, N., and Jiang, D.: Last Glacial Maximum ITCZ Changes From PMIP3/4 Simulations,
895 J. Geophys. Res. Atmos., 128, e2022JD038103, https://doi.org/10.1029/2022JD038103, 2023.

Williams, A. N., Ulm, S., Cook, A. R., Langley, M. C., and Collard, M.: Human refugia in Australia during the Last Glacial Maximum and Terminal Pleistocene: a geospatial analysis of the 25–12 ka Australian archaeological record, J. Archaeol. Sci., 40, 4612-4625, https://doi.org/10.1016/j.jas.2013.06.015, 2013.

900
Wyrwoll, K.-H., and Valdes, P.: Insolation forcing of the Australian monsoon as controls of Pleistocene mega-lake events, Geophys. Res. Lett., 30, 2279, https://doi.org/10.1029/2003GL018486, 2003.

Yan, M., Wang, B., Liu, J., Zhu, A., Ning, L., and Cao, J.: Understanding the Australian Monsoon change during the Last
905 Glacial Maximum with a multi-model ensemble, Clim. Past, 14, 2037–2052, https://doi.org/10.5194/cp-14-2037-2018, 2018.

Yokoyama, Y., Esat, T. M., Thompson, W. G., Thomas, A. L., Webster, J. M., Miyairi, Y., Sawada, C., Aze, T., Matsuzaki, H., Okuno, J., Fallon, S., Braga, J.-C., Humblet, M., Iryu, Y., Potts, D. C., Fujita, K., Suzuki, A., and Kan, H.: Rapid glaciation and a two-step sea level plunge into the Last Glacial Maximum, Nature, 559, 603, https://doi.org/10.1038/s41586-
910 018-0335-4, 2018.

Yukimoto, S., Adachi, Y., Hosaka, M., Sakami, T., Yoshimura, H., Hirabara, M., Tanaka, T., Shindo, E., Tsujino, H., Deushi, M., Mizuta, R., Yabu, S., Obata, A., Nakano, H., Koshiro, T., Ose, T., and Kitoh, A.: MRI-CGCM3 model output

prepared for CMIP5 lgm, served by ESGF, World Data Center for Climate (WDCC) at
915 DKRZ, https://doi.org/10.1594/WDCC/CMIP5.MRMClg, 2015.

Zheng, W., and Yu, Y: Paleoclimate simulations of the mid-Holocene and last glacial maximum by FGOALS, Adv. Atmos. Sci., 30, 684–698, https://doi.org/10.1007/s00376-012-2177-6, 2013.

920 Zhu, J., Otto-Bliesner, B. L., Brady, E. C., Poulsen, C. J., Tierney, J. E., Lofverstrom, M., and DiNezio, P.: Assessment of equilibrium climate sensitivity of the Community Earth System Model version 2 through simulation of the Last Glacial Maximum, Geophys. Res. Lett., 48, https://doi.org/10.1029/2020GL091220, 2021.

Zhu, J., Otto-Bliesner, B. L., Brady, E. C., Gettelman, A., Bacmeister, J. T., Neale, R. B., Poulsen, C. J., Shaw, J. K.,
925 McGraw, Z. S., and Kay, J. E.: LGM Paleoclimate Constraints Inform Cloud Parameterizations and Equilibrium Climate Sensitivity in CESM2, J. Adv. Model. Earth Syst., 14, e2021MS002776. https://doi.org/10.1029/2021MS002776, 2022.